UNIVERSIDAD DE MÁLAGA

E.T.S. INGENIERÍA INFORMÁTICA
UNIVERSIDAD DE MÁLAGA

Grado en Ingeniería de la Salud

Caracterización matemática de factores implicados en la aparición de la siringomielia en condiciones de ingravidez

Mathematical characterization of factors involved in the occurrence of syringomyelia under weightless conditions

Realizado por

María Torés España

Tutorizado por

Víctor Smith Fernández *

Cotutorizado por

Luis Parras Anguita **

Departamento

Área de Anatomía y Embriología Humana *
Ingeniería Mecánica, Térmica y de Fluidos **

MÁLAGA, junio de 2023

ESCUELA TÉCNICA SUPERIOR DE INGENIERÍA INFORMÁTICA

GRADO EN INGENIERÍA DE LA SALUD

Caracterización matemática de factores implicados en la aparición de la siringomielia en condiciones de ingravidez

Mathematical characterization of factors involved in the occurrence of syringomyelia under weightless conditions

Realizado por
María Torés España
Tutorizado por
Víctor Smith Fernández *
Co-tutorizado por
Luis Parras Anguita **
Departamento
Área de Anatomía y Embriología Humana *
Ingeniería Mecánica, Térmica y de Fluidos **
UNIVERSIDAD DE MÁLAGA
MÁLAGA, JUNIO DE 2023

Fecha defensa: junio de 2023

Resumen

Este proyecto de fin de grado tiene como objetivo caracterizar el flujo y comportamiento del líquido cefalorraquídeo (CSF) bajo la influencia de la gravedad. Simulamos condiciones normales y de ingravidez para comparar y analizar los resultados.

Material y métodos: Para este proyecto de investigación, se utilizaron imágenes de resonancia magnética (MRI) para crear un modelo 3D que representara el espacio del líquido cefalorraquídeo (CSF), el propio líquido y la médula espinal para su posterior análisis mediante los programas Ansys Fluent, Structural Transient y Matlab. Para la segmentación de imágenes, se utilizó el programa 3D Slicer, mientras que para mejorar el modelo se utilizaron MeshLab y Spaceclaim. En cuanto al análisis, se utilizó Ansys Fluent para el estudio del flujo del CSF, Structural Transient para el estudio de la deformación de la médula espinal, y Matlab para el procesamiento de datos y la obtención de resultados numéricos.

Resultados: La distribución de presión a lo largo de la médula espinal mostró un cambio gradual de una presión alta a una presión baja, mientras que la duramadre presentó una distribución de presión relativamente constante. El modelo que simulaba la siringomielia mostró una interrupción en el flujo del líquido cefalorraquídeo (LCR), caracterizada por obstrucción y cambios en las trayectorias, reflejando la anatomía realista de la médula espinal. Además, el modelo que simulaba la siringomielia exhibió una deformación visual más pronunciada, con un notable aumento de tamaño y una mayor tensión en la parte inferior. El análisis del caudal reveló variaciones cíclicas en los flujos de entrada y salida, reflejando el equilibrio dinámico del transporte del LCR

Conclusiones: Nuestro estudio ha contribuido a una mejor comprensión de las complejas interacciones biomecánicas entre la médula espinal y el líquido cefalorraquídeo (LCR). Hemos obtenido datos significativos sobre la distribución de presión, el esfuerzo cortante, la deformación y la dinámica del flujo dentro de la médula espinal mediante la combinación de simulaciones computacionales con métodos de visualización. Nuestros hallazgos también destacan la importancia de considerar el canal central al estudiar el flujo del LCR y su impacto en la función de la médula espinal.

Palabras claves: ANSYS, líquido cefalorraquídeo, interacción fluido-estructura, siringomielia

Abstract

This final year project dissertation aims to characterize the flow and behaviour of cerebrospinal fluid (CSF) under the influence of gravity. We simulated both normal and weightless conditions to compare and analyse the results. The modelling allowed us to determine the circumstances under which the spinal canal tends to close.

Material and methods: We used magnetic resonance imaging (MRI) images to create a three-dimensional model of the cerebrospinal fluid (CSF) space, CSF, and spinal cord. The model was subsequently analysed using ANSYS Fluent, ANSYS Structural Transient, and MATLAB. We used 3D Slicer for image segmentation, MeshLab and SpaceClaim for model refinement. ANSYS Fluent was used for computational fluid dynamics simulations to characterize CSF flow, pressure gradients, and deformation in both normal and weightless conditions. ANSYS Structural Transient was used for finite element analysis to investigate the mechanical behaviour of the spinal cord under different gravitational conditions. Finally, MATLAB was utilized for data analysis.

Results: The pressure distribution along the spinal cord showed a decreasing gradient from high to low pressure, while the duramater exhibited a relatively consistent pressure distribution. The model with the central canal and syrinx demonstrated disrupted CSF flow, characterized by obstruction and altered pathlines, reflecting the realistic anatomy of the spinal cord. The model with the syrinx displayed greater visual deformation, with noticeable enlargement and a higher strain at the bottom. The mass flow rate analysis revealed cyclic variations in the inlet and outlet flows, reflecting the dynamic balance of CSF transport.

Conclusion: Our study has contributed to a better understanding of the complicated biomechanical interactions between the spinal cord and cerebrospinal fluid (CSF). We have obtained significant data on the distribution of pressure, shear stress, deformation, and flow dynamics within the spinal cord by combining both computational simulations with visualisation methods. Our findings also emphasize the significance of considering the central canal when studying CSF flow and its impact on spinal cord function.

Keywords: ANSYS, cerebrospinal Fluid, Fluid–structure interaction, syringomyelia

To my parents for paying for all the necessary tuition to get here. Without your sacrifices and encouragement, I would not be where I am today. Thank you from the bottom of my heart.

To Edu, for helping me out.

To my tutors, for the time dedicated.

To Tomás, my high school teacher, for believing in me when no one else did.

And last but not least, to Ewan, because without your support, I would not have made it this far.

Contents

1. Introduction 1

1.1 Epidemiology 1
1.2 Motivation 1
1.3 Goals 2
2. State of the Art 3

2.1 Background 3
2.1.1 Cerebrospinal fluid 3

2.1.1.1 Anatomical characterization 3

2.1.1.2 Physiological characterization 6

2.1.1.3 Dynamics of the CSF 6

2.1.2 Chiari Malformation 7

2.1.3 Syringomyelia 8

2.1.3.1 Revisited hydrodynamic theory 10

3. Materials and methods 13

3.1 Image acquisition 14
3.2 Image segmentation 14
3.3 Geometry reconstruction 15
3.4 3D geometry preparation 16
3.5 Fluids-structure interaction (FSI) simulation 17
3.5.1 Ansys Fluent 18

3.5.2 Transient Structural Module 21

3.6 Updates for Central Canal and Syrinx Incorporation 23
3.6.1 Modelling the Central Canal 23

3.6.2 Modelling the syrinx 25

4. Results 29

4.1 Weightless conditions 29
4.1.1 CSF-Spinal Cord Model 29

4.1.1.1 Pressure 30

4.1.1.2 Velocity Vectors 30
4.1.1.3 Streamlines 32
4.1.1.4 Wall Shear Stress 32
4.1.1.5 Deformation 34
4.1.1.6 Shear Stress Deformation 34
4.1.2 CSF-Spinal Cord-Central Canal Model 35
4.1.2.1 Pressure 35
4.1.2.2 Velocity vectors 36
4.1.2.3 Streamlines 37
4.1.2.4 Wall Shear Stress 38
4.1.2.5 Deformation 39
4.1.2.6 Shear Stress Deformation 39
4.1.3 CSF-Spinal Cord-Central Canal-Syrinx Model 40
4.1.3.1 Pressure 40
4.1.3.2 Velocity Vectors 42
4.1.3.3 Pathlines 42
4.1.3.4 Wall Shear Stress 42
4.1.3.5 Deformation 44
4.1.3.6 Wall Shear Deformation 45
4.3 MATLAB graphics 46
5. Discussion 51
5.1 Limitations 52
6. Conclusions 53
6.1 Future lines of research 53
7. Conclusiones 55
7.1 Futuras líneas de trabajo 55
Bibliography 57
Appendix 63

List of Figures

Figure 2.1 (Orešković et al., 2017): Image showing the Cerebrospinal Fluid System 4
Figure 2.2 (Cousins et al., 2021): Ventricular System-Pathway of the CSF flow..... 4
Figure 2.3 (Zahid et al., 2021): CSF flow rate vs. time over a cardiac cycle, with descriptions of flow and pulsatility variables shown..... 7
Figure 2.4 (Chiari Malformation: Non-surgical Alternatives to Chiari Decompression Surgery – Caring Medical Florida, n.d.): Image showing normal (A) and Chiari I malformation with syrinx (B)..... 8
Figure 2.5: (Pillay et al., 1992)..... 11
Figure 2.6. (Pillay et al., 1992)..... 11
Figure 3.1: CFD diagram 13
Figure 3.2: MR image in all three planes (axial, coronal and sagittal) 14
Figure 3.3: Spaceclaim geometry model..... 16
Figure 3.4: (Ma et al., 2020). One-way FSI approach diagram 17
Figure 3.5: Project Schematic of the analysis on ANSYS workbench..... 18
Figure 3.6: Polyhedral mesh on Watertight Geometry workflow, Ansys Fluent..... 18
Figure 3.7: Sinusoidal Velocity Profile for Cerebrospinal Fluid (CSF) in Flow Simulation ... 21
Figure 3.8: Graphical representation of the mesh and boundary conditions on Transient Structure Module..... 23
Figure 3.9: Image of the small cylindrical structure representing the central canal 24
Figure 3.10: Three-dimensional model of cerebrospinal fluid space, spinal cord, and central canal 24
Figure 3.11: Mesh Visualization of CSF Space, Spinal Cord, and Central Canal Model with Z-Axis Cut..... 25
Figure 3.12: Mesh Visualization of CSF Space, Spinal Cord, and Central Canal Model with X-Axis Cut..... 25
..... 26
Figure 3.13: Visualization of syrinx within the spinal cord 26
Figure 3.14: 3D Mesh Model of Spinal Cord with Syrinx Inside Central Canal and cut in Z-Axis 27
Figure 4.1: Pressure gradients [Pa]: (A) Spinal cord (B) Duramater 30

Figure 4.2: Velocity vector plot of the CSF coloured by velocity magnitude. 31
Figure 4.3: Zoom of the velocity arrows. 31
Figure 4.4: Streamlines coloured by velocity of the CSF 32
Figure 4.5: Shear stress contour on the dura mater tissue 33
Figure 4.6: Wall Shear stress contour of the spinal cord 33
Figure 4.7: Structural Deformation of the Spinal Cord in Response to Pressure Gradient Changes in Cerebrospinal Fluid Flow under weightless conditions 34
Figure 4.8: Visualization of Shear Stress Contours and Deformations in a Spinal Model 35
Figure 4.9: A. Image showing pressure distribution for the spinal cord. B . Image showing pressure distribution for the duramater tissue 36
Figure 4.10: Velocity Vectors: Normal and Zoomed-In Views 37
Figure 4.11: Fluid Pathlines in Spinal Cord Model with Central Canal 38
..... 38
Figure 4.12: A. Wall Shear Stress Distribution in Spinal Cord Model with Central Canal. B. Wall Shear Stress Distribution in the duramater tissue 38
Figure 4.13:Deformation of Spinal Cord Model with Central Canal 39
Figure 4.14: Wall Shear Deformation on XZ-Axis in Spinal Cord Model with central canal . 40
Figure 4.15: Image showing pressure distribution for the spinal cord & syrinx model. A. Spinal Cord. B. Duramater tissue 41
Figure 4.16: Pressure gradient distribution at top and bottom of syrinx 41
Figure 4.17: Pathlines of Flow Through Spinal Canal with Syrinx Obstruction 42
Figure 4.18: Wall Shear Stress Distribution in Spinal Cord with Syrinx Obstruction 43
Figure 4.19: Wall Shear Stress Distribution on Synrinx Obstructing Central Canal 43
Figure 4.20: Deformation of Spinal Cord Model with Central Canal and Syrinx 44
Figure 4.21: Deformation Simulation of Syrinx in the Spinal Cord 45
Figure 4.22: Visualization of Wall Shear Strain Distribution in the spinal cord 45
Figure 4.23: Visualization of Wall Shear Strain Distribution in Syrinx 46
Figure 4.24: Mass Flow Rate results 46
Figure 4.25: Mass Flow Rate Variation in CSF Flow Simulation: Inlet 47
Figure 4.26: Mass Flow Rate Variation in CSF Flow Simulation: Outlet 47
Figure 4.27: Net Flow Variation 48
Figure 4.28: Area results 49
Figure 4.29: Surface Areas of Different Components in CSF Flow System 49

List of Tables

Table 2.1: Classification of syringomyelia.....9
Table 3.1: Software usage pathway and procedures.....13
Table 3.2: Boundary conditions.....19
Table 3.3 (A Poroelastic Model of Spinal Cord Cavities, n.d.): Material properties.....21
Table 3.4 (Liu et al., 2017): Boundary conditions on Ansys Fluent.....21
Table 3.5 (A Poroelastic Model of Spinal Cord Cavities, n.d.): Bulk system material properties 22
Table 3.6 (Martin et al., 2005), (Rusbridge et al., 2006): Mechanical Properties of Syrinx Cavities.....26

1

Introduction

This study investigates the biomechanics of cerebrospinal fluid (CSF), with a focus on syringomyelia.

It entails simulating the tissue and fluid of the spinal cord as well as its surroundings.

1.1 Epidemiology

The cerebrospinal fluid (CSF) is a colourless ultrafiltrate of plasma with a low content of cells and proteins (Di Terlizzi & Platt, 2006). The CSF is mainly produced by the choroid plexuses, running through the entire cerebral ventricular system, and flowing out to the subarachnoid spaces through openings in the fourth ventricle called the foramens of Luschka and Magendie. Thanks to this, the CSF envelops every single cavity of the encephalon and spinal cord (Haynes, 2019).

Syringomyelia is neurological disorder related to flow alterations within the CSF. It is caused by the presence of an intra-medullary cyst in the spinal cord, mostly as a result of either Chiari-1-malformation or severe spinal trauma (Stienen et al., 2011) that due to pressure differences can result in fluid being sucked from the ventricles into the central canal (Sternberg & Gunter, 2017).

Studies have shown that at least 28% of spinal cord injured patients develop a syrinx (fluid-filled cavities). However, alternatives for treatment are very restricted and only less than 50% of the patients who are treated show any improvements (Kyriakou, 2006).

1.2 Motivation

Gravity has a strong impact on fluid distribution and pressure within the human circulation, so different gravity conditions can reduce or increase central venous and intracranial pressure (Lawley et al., 2017). Formation of strong gravitational pressure waves in the presence of craniospinal pressure dissociation causes syringomyelia. Hypothetically, the cranial space works as a shock absorber for the long vertical lumbar space, if this space is cut off the CSF pressure waves may arise. When gravitational waves form along the spinal cord the probability

of syrinx formation increases, as the spinal cord may be physically delimited along the normally closed central canal (Cinalli et al., 2019).

The CSF is not easily accessible for in vivo measurements (unless invasive implementation of measurement devices are used) so evaluating how different gravity and pressure parameters impact its behaviour is challenging (Dai et al., 2020).

This is why acquiring a better understanding of CSF dynamics and the role that those variables play is necessary if we want to come up with better treatments.

1.3 Goals

With this dissertation we aim to:

- Use a numerical model to characterize the flow and behaviour of the CSF under normal and weightless conditions.
- Study the effect that gravity has in the development of syringomyelia by implementing a computational model that simulates the spinal canal under normal and weightless conditions.

2

State of the Art

2.1 Background

This chapter introduces the theorical background of our dissertation, as well as the basic knowledge needed to fully understand the rest of the study.

2.1.1 Cerebrospinal fluid

2.1.1.1 Anatomical characterization

The anatomy of the cerebrospinal fluid system includes the cerebral ventricles as well as the spinal and brain subarachnoid spaces, cisterns and sulci.

The CSF is produced mainly but not exclusively by the choroid plexuses, mostly in the lateral ventricles. The CSF passes through the interventricular foramen of Monro, into the third ventricle. It exits the third ventricle through the cerebral aqueduct of Sylvius into the fourth ventricle and it continues into the central canal of the spinal cord through the obex. It flows out the fourth ventricle into the spinal subarachnoid space through the median aperture of Magendie and the two lateral apertures of Luschka, ultimately being absorbed into the venous blood at the level of the arachnoid granulations (see figure 2.1 and 2.2) (Brinker, 2014) (Adigun & Al-Dhahir, 2019).

In comparison to blood plasma, the CSF has a higher concentration of chloride, magnesium and sodium besides showing a lower amount of potassium, glucose, proteins, albumin and uric acid (Haynes, 2019).

CSF pressure is regulated primarily by its absorption through the arachnoid granulations. The rate of CSF formation is very constant, and so this process is rarely a factor in pressure control (Di Terlizzi & Platt, 2006). For humans, normal CSF pressure changes between 8 mmHg to15 mmHg supine and about 20 mmHg erect (Adigun & Al-Dhahir, 2019).

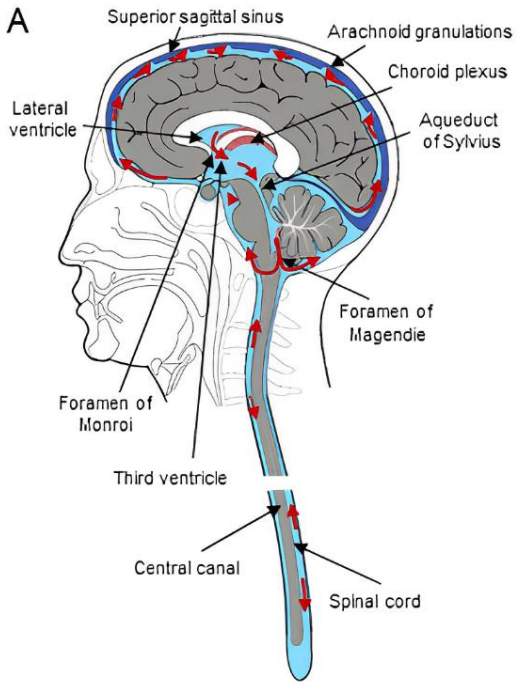

Figure 2.1 (Orešković et al., 2017): Image showing the Cerebrospinal Fluid System

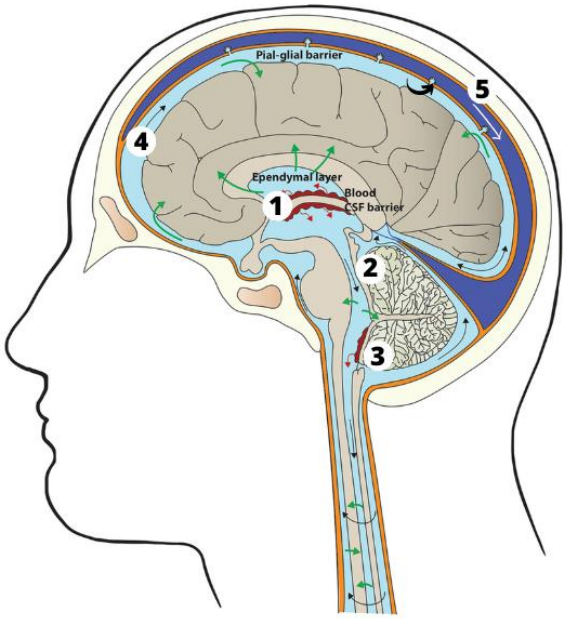

Figure 2.2 (Cousins et al., 2021): Ventricular System-Pathway of the CSF flow

There are three possible spaces through which CSF can enter the interior of the spinal cord and form CSF cysts due to their different porosity values:

- Ependymal cells

Ependymal cells are specialized epithelial cells that cover the brain's ventricles and the spinal cord's central canal. They are necessary for producing, circulating, and absorbing cerebrospinal fluid (CSF) (Deng et al., 2022)

The ependymal cells play a key role in maintaining the spinal cord parenchyma. They build a barrier that separates the CSF from the tissue. This barrier consists of tight unions between ependymal cells that create a seal (Nelles & Hazrati, 2022).

Besides their barrier function, ependymal cells are also involved in the regulation of CSF flow and composition. They possess motile cilia that beat in a coordinated motion, creating a directional flow of CSF along the spinal cord. This flow helps to remove waste products and maintain a stable environment (Kumar et al., 2021).

However, in certain pathological conditions, such as syringomyelia, the ependymal barrier may become affected, they become unable to maintain the barrier function, allowing CSF to enter the surrounding tissue and form cysts (Jiménez et al., 2014)

- Virchow-Robin spaces

The Virchow-Robin spaces are perivascular spaces that surround arterioles as they penetrate into the brain and spinal cord. These spaces are lined by a layer of pia mater and filled with cerebrospinal fluid (CSF). In some cases, the Virchow-Robin spaces can become enlarged and form cysts that are known as perivascular cysts (Fanous & Midia, 2007)

One proposed mechanism is that the enlargement of the Virchow-Robin spaces may cause compression of the nearby spinal cord tissue, leading to the formation of a syrinx. Another proposed mechanism is that the perivascular cysts may disrupt the flow of CSF, leading to the accumulation of fluid within the spinal cord and the development of a syrinx (Stoodley et al., 2000)

- Spinal subarachnoid space

Between the pia mater and the arachnoid mater, which surrounds the spinal cord, is a region called the spinal subarachnoid space that is filled with fluid. CSF fills both of them, which are connected to the brain's subarachnoid region. (Shafique, 2022)

A cyst may develop if the CSF flow is blocked for a variety of reasons, such as spinal cord tumours, injuries to the spinal cord, and other disorders that cause the spinal cord to be compressed in the subarachnoid space (Farb & Rovira, 2020)

Cysts might also develop because of changes to the CSF's pressure dynamics. For instance, fluid may flow into the cyst and cause it to enlarge if there is an imbalance of pressure between the subarachnoid space and the cyst (National Organization for Rare Disorders, 2023)

2.1.1.2 Physiological characterization

The CSF serves a great deal of purposes. Some of them can easily be listed:

- It has a protective role. It protects the encephalon from fluctuations in the arterial and central venous pressures related to posture and movement (Bailey and Vernau, 1997)
- It oversees the excretion of potentially toxic substances product of the cerebral metabolism.
- It works as a filter to allow the movement of water-soluble substances from the brain parenchyma (Di Terlizzi, R., & Platt, S, 2006).
- It is in charge of the intracerebral transport of active substances (Di Terlizzi, R., & Platt, S, 2006)
- It provides hydromechanical protection (Telano, L. N., & Baker, S. 2022):
    - CSF acts as a shock absorber, cushioning the brain against the skull.
    - It serves buoyancy. CSF creates a floating effect on the CNS. The weight of the brain varies with CSF: 50 g when it is submerged in the CSF and 1400 g when it is not (Idris, 2014).

2.1.1.3 Dynamics of the CSF

CSF movement is essential because, as it has been stated in the previous section, the CSF oversees many vital functions that in the end are responsible of the homeostasis of the central nervous system.

The CSF movement is an active process that happens as a consequence of different physiological processes. Mostly due to the ciliary movement of ependymal cells, pressure difference between choroid plexuses, subarachnoid granulations, arteries pulsations in the subarachnoid space and arterioles of Virchow spaces as well as passive movement of CSF through the ependyma and telencephalons and spinal cord movement during normal activity (Haynes, 2023).

CSF flow is pulsatile (see figure 2.3), created by the Windkessel effect. Both the cardiac and the respiratory cycles have been suggested as CSF flow drivers even though it seems to be predominantly driven by the cardiac cycle. The artery wall's pace matches that of the CSF, implying that arterial wall motion is the primary driving mechanism, via a process known as perivascular pumping. Raising blood pressure does not modify the artery diameter but alters the pulsations of the arterial wall, increasing backflow and reducing net flow in the perivascular spaces (Mestre, 2018).

During systole, the cranial arteries expand, causing the middle and lower portions of the brain to swell and causing CSF pulsations at the FM in a caudal direction into the spinal canal. CSF will flow in the cranial direction to compensate for volume conservation when blood flows away from the skull during diastole. Moreover, when blood volume inside the skull grows, so does intracranial pressure. This pressure forces the CSF into the spinal canal (Greitz et al., 1992).

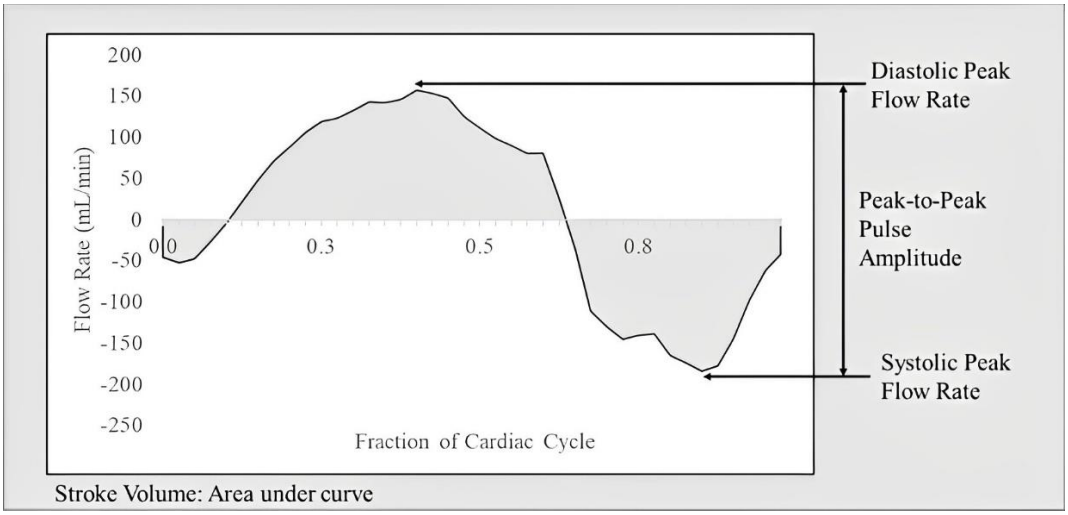

Figure 2.3 (Zahid et al., 2021): CSF flow rate vs. time over a cardiac cycle, with descriptions of flow and pulsatility variables shown.

2.1.2 Chiari Malformation

A Chiari malformation occurs when the bottom section of the brain protrudes into the spinal canal. There are four major varieties, with Chiari I being the most frequent.

The lowest section of the back of the brain spreads into the spinal canal in people with Chiari I. This can place pressure on the brainstem and spinal cord, as well as block fluid flow (NHS website, 2022).

Syrinx cavities are most typically linked with Chiari abnormalities, creating a partial CSF flow restriction in the spinal subarachnoid space (Holly & Batzdorf, 2019).

Chiari malformation (see figure 2.4) is the most common cause of syringomyelia, while the exact etiology is unknown. It is hypothesized to be caused by cerebellar tissue impeding flow at the foramen magnum, which interferes with the normal CSF pulsations that were mentioned before (Chiari Malformation – Symptoms, Diagnosis and Treatments, n.d.).

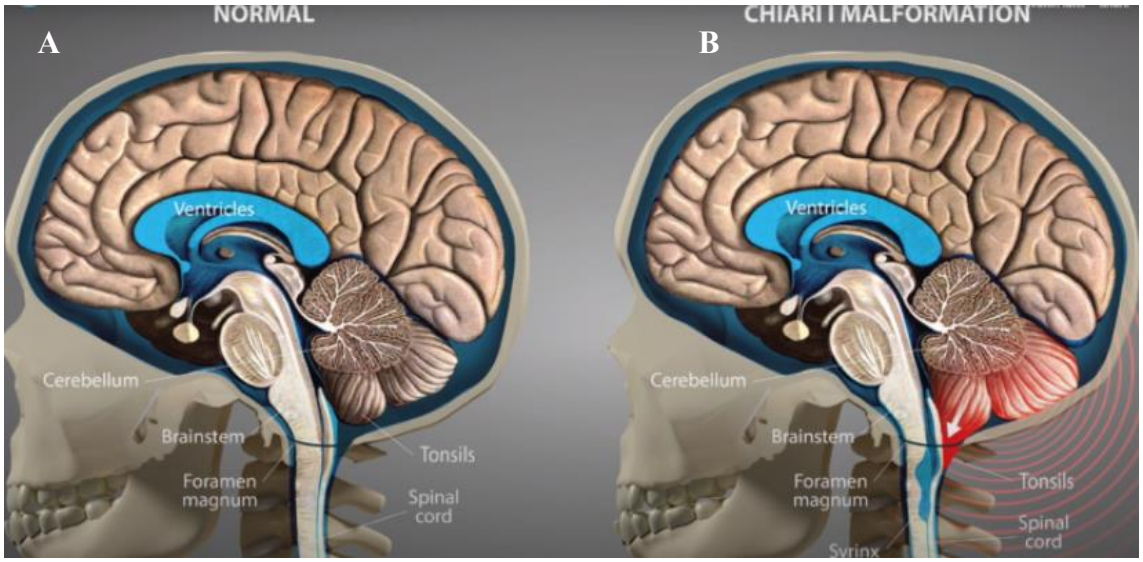

Figure 2.4 (Chiari Malformation: Non-surgical Alternatives to Chiari Decompression Surgery – Caring Medical Florida, n.d.): Image showing normal (A) and Chiari I malformation with syrinx (B)

2.1.3 Syringomyelia

Syringomyelia (SM) is a condition in which a cyst forms and grows within the spinal cord. The enlarging syrinx slowly deteriorates the cord, causing paresthesia, discomfort, weakness, and stiffness of the trunk, shoulders, arms, or legs. Sweating, sexual function, bladder and bowel control may also be affected (Verhaagen & McDonald, 2012).

It basically consists on disruptions in cerebrospinal fluid (CSF) flow in the subarachnoid spaces alter flow velocity resulting in the syrinx (Leclerc et al., 2021).

Syringomyelia most usually affects the cervical and upper thoracic spinal cord, although it can affect the entire spinal cord (Squire, 2008) which helps us justify why we will be only modelling this region later on.

The three major types of syringomyelia are due to (Squire, 2008):

- Congenital brain defects: Chiari I malformation is the most common cause of syringomyelia. Chiari I malformation is considered congenital in the majority of individuals. However, after lumbar or ventricular shunting, Chiari I malformation can occur.
- Injury to the spinal cord: Other disorders that may be linked with syringomyelia include spinal cord tumours, spinal arachnoid cysts, traumatic paraplegia, postinfectious or post inflammatory meningitis, and so on.

And therefore, can be classified as (Syringomyelia, 2022):

- Communicating syringomyelia- or foraminal refers to cavities that communicate directly with the fourth ventricle via the obex are generally linked with hindbrain abnormalities.
- Non-Communicating syringomyelia- or nonforaminal refers to cavities without contact with the fourth ventricle and is frequently caused by trauma and spinal cord tumours, although it is also linked to hindbrain abnormalities.

Merging all of this, the current classification distinguishes:

Classification	Pathogeny	Etiologies
Foraminal syringomyelia	Hindbrain pathologies	Chiari malformation I/II
	Non hindbrain pathology	Forminal arachnoiditis
		Hydrocephalus
Non-Foraminal syringomyelia	Arachnoiditis	Spine trauma
		Infections
		Herniated disc
		Spinal arachnoid cyst
		Tethered cord
		Tumours

Table 2.1: Classification of syringomyelia

2.1.3.1 Revisited hydrodynamic theory

According to Poiseuille's law, laminar flow through a tube is inversely proportional to the fourth power of the radius. As a result, a decrease in vessel diameter results in a four-fold increase in resistance. If any pressure increase caused by an increase in CNS volume is dispersed across the intrathecal space, the average diameter of numerous veins will be reduced. If a CNS volume increase affects the whole CNS venous system, the overall reduction in venous outflow is minimised, and hence free flow of CSF helps venous drainage. Since the flow of CSF with gravitational force allows both fluids to encounter the same pressure gradient, veins inside the head do not collapse when shifting to an upright position. CSF flow obstruction in the foramen magnum is a major cause of poor compliance. While movement appears to contribute to foramen magnum occlusion, CSF flow may be altered by posture. The head and spine can be temporarily divided into sections with lower pressure volume indices. Obstruction may be present even if there is no evident hindbrain hernia or cerebellar malformation. Normally, pressure gradients between the CSF compartments of the head and spine are caused by gravity. Pressure in the head and spine may change independently in the presence of a blockage caused by spina bifida or syringomyelia. This condition is known as "craniospinal pressure dissociation." (Williams, 2008).

When referring to "craniospinal pressure dissociation", perhaps the most convincing evidence is that in patients with communicating syringomyelia, there is always an irregularity of such type, in which a pressure difference can be assumed, and measured, between the area from which the CSF came and the region to which it flows. As a result, the typical scenario is high pressure in the skull and low pressure in the spine (B. Williams, 1980).

Gardner's hydrodynamic theory is one of several proposed theories for the incidence of syringomyelia. Gardner ascribed the development of syringomyelia to craniospinal pressure differentials in the presence of fourth ventricular outlet blockage; these differentials encourage cerebrospinal fluid movements from the brain's fourth ventricle to the spinal cord's central canal (Pillay et al., 1992).

A proposed more accurate unified theory (see figure 2.6) of syringomyelia includes three theories (see figure 2.5): Gardner's hydrodynamic theory, Gardner's hydrodynamic theory with refinements introduced by Williams and theories of Ball and Dayan and Aboulker (Pillay et al., 1992).

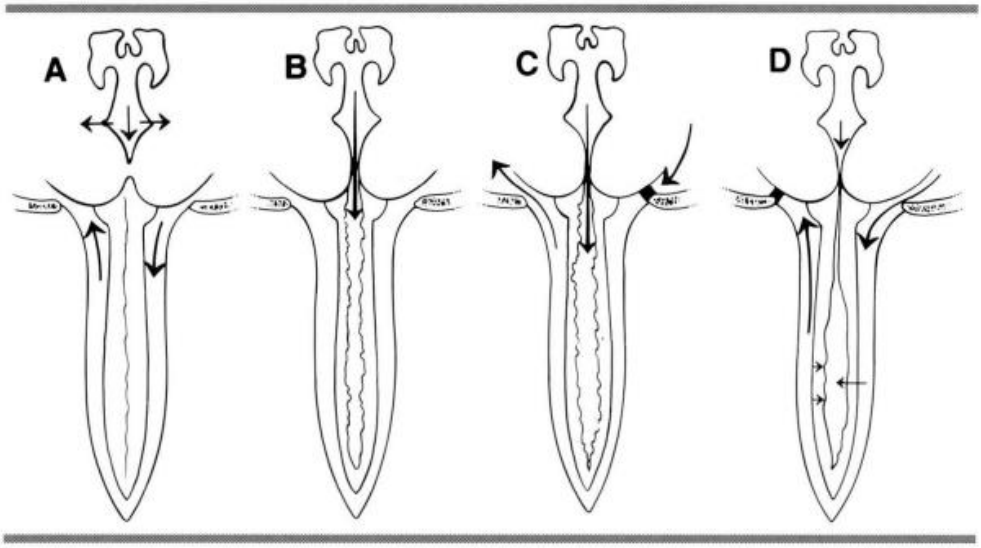

Figure 2.5: (Pillay et al., 1992). A, normal cerebrospinal fluid dynamics, with tiny arrows indicating free flow via fourth ventricle outputs and big arrows suggesting free flow around the craniocervical junction. B, Gardner's hydrodynamic hypothesis, in which a blockage of the fourth ventricle outflow directs the cerebrospinal fluid pulse wave through the obex into the spinal cord's central canal, resulting in a syrinx. C, Williams' hypothesis, according to which foramen magnum blockage causes the establishment of a craniospinal pressure gradient, resulting in hindbrain impaction and syrinx formation. D, the Ball, Dayan, and Aboulker hypotheses, according to which foramen magnum disease causes increased intraspinal pressure, pushing fluid into the spinal cord via the Virchow-Robin gaps or nerve roots.

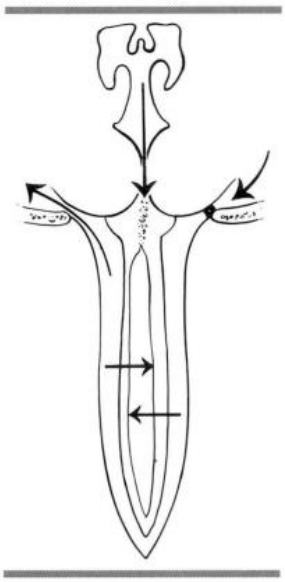

Figure 2.6. (Pillay et al., 1992). A proposed unified theory of syringomyelia concludes that Gardner's hydrodynamic forces are increased in the setting foramen magnum occlusion as William stated. Transparenchymal fluid migrations (as proposed by Ball and Dayan and Aboulker) might explain syringe coalescence and propagation, as well as localised posttraumatic syringomyelia unrelated to hindbrain disease.

3

Materials and methods

Learning about the cerebrospinal fluid and its interaction with brain tissues is a key step towards understanding the origins of many disorders in the central nervous system. An elastic finite element model has been developed to investigate mechanisms in the lead prior to syrinx formation.

Three separate 3D models of the spinal cord and the spinal subarachnoid space (SAS) have been built using MRI anatomical images.

In this chapter, the whole process is precisely described including descriptions of steps for the used software (see figure 3.1).

Description	Software	Export
Image acquisition	-	DICOM
Image segmentation	3D Slicer	.stl
3D geometry reconstruction	MeshLab	.stl
3D geometry preparation	SpaceClaim	.scdoc
FSI simulation	Ansys Fluent, Structural Transient	EnSight files

Table 3.1: Software usage pathway and procedures

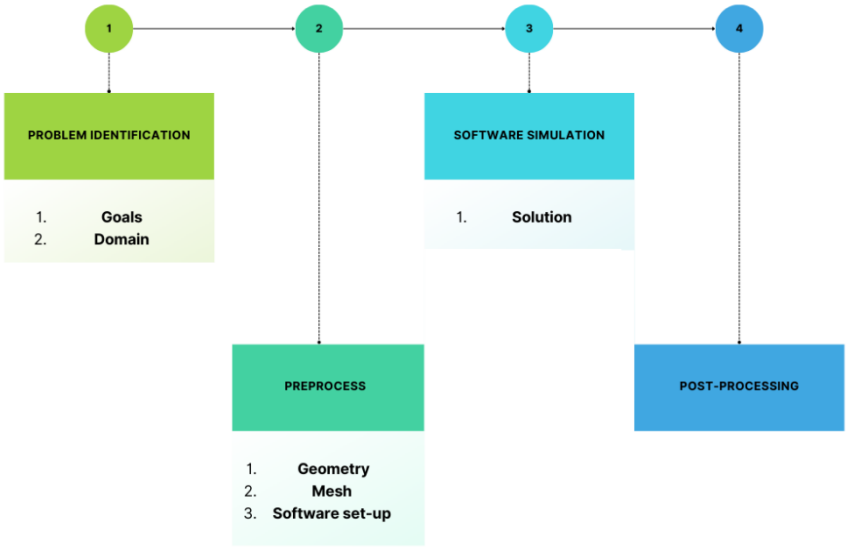

Figure 3.1: CFD diagram

3.1 Image acquisition

Three separate 3D models of the spinal cord and the SAS have been built using MRI anatomical images (see figure 3.2).

3.2 Image segmentation

For the image segmentation commercial software 3D Slicer was used. It is a semi-automatic method, so it is necessary that the image quality is sufficient. In this case we used some of the MRI samples that the software provides.

Segmentation was done for the spinal cord and the SAS in two different models. They both extend from approximately the foreman magnum to the C3 bone in the sagittal plane.

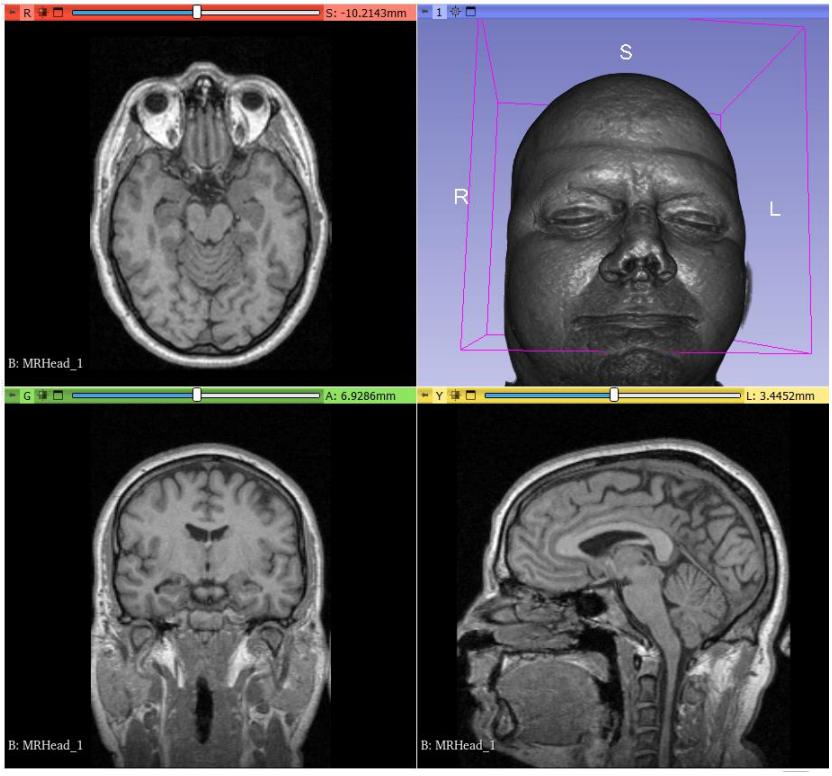

Figure 3.2: MR image in all three planes (axial, coronal and sagittal)

The segmentation was achieved by first manually outlining the boundaries of the spinal subarachnoid space and spinal cord on the three planes.

- MRI images were opened by 3D Slicer from “File >> Download sample data”
- Semi-automatic segmentation was done using “Segment Editor >> Paint >> Sphere brush” by selecting it from “Modules”.

- Segmented model was exported as ".stl" file format from "Segmentation >> Export models >> Export to files…"

Once segmented, the 3D model of the CSF space was exported in (.stl) format for simulation purposes.

3.3 Geometry reconstruction

Two distinct software were used to rebuild and prepare the 3D model. For reconstructing and smoothing we move onto MeshLab as it offers a wide variety of cleaning, repairing and reconstructing tools for our mesh.

The Surface Reconstruction: Screen Poisson filter was used to solve the missing vertices and hole issues.

Smoothing was applied to remove pixelation artifacts using by the Laplacian smoothing algorithm (which has smoothing steps of 10, with 1D Boundary smoothing and cotangent weighting)

- Cleaning and repairing were applied in MeshLab from: "Filters >> Cleaning and Repairing >> Merge close vertices >> Remove duplicate vertices >> Remove faces >> Remove unreferenced vertices >> Repair non manifold edges"
- Surface reconstruction was applied from: "Filters >> Remeshing, Simplification and Reconstruction >> Surface Reconstruction: Screen Poisson".
    - Reconstruction depth [12]
- Smoothing was applied from "Filters >> smoothing, Fairing and Deformation >> Laplacian Smooth" and activating the following:
    - Smoothing steps [10]
    - 1D Boundary Smoothing
    - cotangent weighting
- Exporting the file as (.stl) from "File >> Export Mesh As… >> STL File Format (*.stl)"

NOTE: Simplification: Quadric Edge Collapse Decimation was used to reduce the vertex count of the mesh for reduced file size.

3.4 3D geometry preparation

For this next step, software Spaceclaim will be used so we can obtain a final geometry model (see figure 3.3).

- Planes are set on what will be the entrance and exit of our model. The purpose of this is to help us define our inlet and outlet later.
- We use the tool *Shrink Wrap* to smooth over some roughness and soften the edges that will help with the next operation from "Facets >> Shrink Wrap".
- We select the *Autoskin* option which allows us to create surface patches from the faceted data. In other words, it helps us to extract surface or solid geometry from a STL file. "Tools >> Autoskin"
- Once this process is over, we go back to the planes that we had stablished before and with the help of the moving tool, we will slide it down and proceed to cut it. By doing this we are achieving flat surfaces that are easy to work with and get a piece of geometry that we can take into meshing.
- In order to define our surfaces: "Groups>> Create new NS >> Select faces >> WALL" (this very same step is done for the entrance, exit and internal wall)

The process is done with the two 3D models that we previously obtained.

- Once they are both ready, we proceed to assemble them together: "Assembly >> File"
- Exporting the file as (.scdoc) from "File >> Save as…"

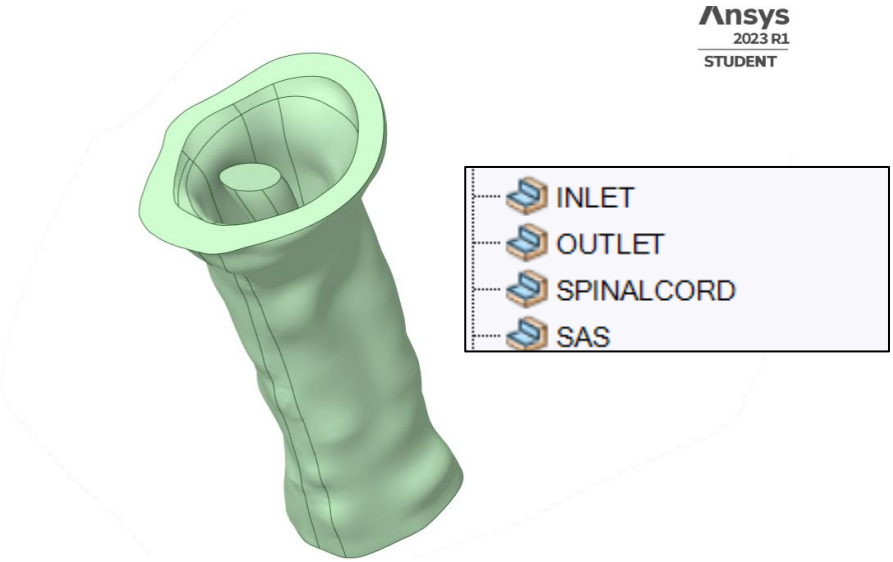

Figure 3.3: Spaceclaim geometry model

3.5 Fluid-structure interaction (FSI) simulation

When fluid flow interacts with a solid body and exerts pressure, FSI can be employed. This pressure generates a force, which leads to solid deformations and, as a result, produces a displacement of the CSF (see figure 3.4). When deformations on the fluid side are ignored, a one-way approach is implemented.

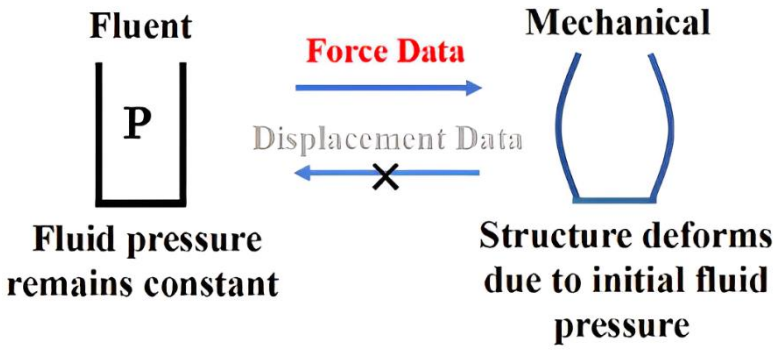

Figure 3.4: (Ma et al., 2020). One-way FSI approach diagram

FSI simulations in both models were carried out by simultaneously running ANSYS fluent and ANSYS Mechanical (Multiphysics problem). To solve these equations, the algorithm employs a finite volume technique with constrained second order differencing in both space and time. Unstructured polyhedral components were used to mesh the models.

Because it is a one-way FSI elastic model, the effects of the CSF pressure on tissue stress are shown. The model was used to determine stress and pressure in the cord prior to syringomyelia cavity development.

ANSYS workbench software was used to solve the one-way coupling of the fluid and solid domains (see figure 3.5).

By using the coupled system in FSI simulations, we can get a more accurate representation of the physical phenomena being modelled, as it takes into account the interactions between the fluid and solid regions.

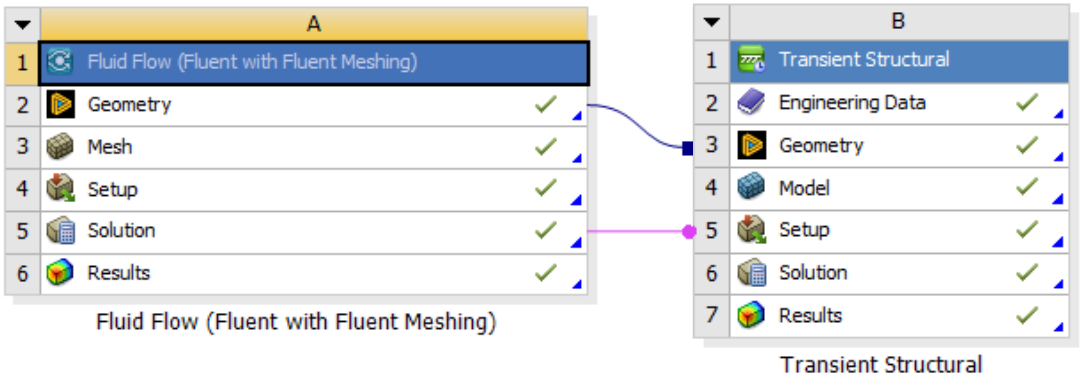

Figure 3.5: Project Schematic of the analy.

3.5.1 Ansys Fluent

A one-way FSI simulation basically consists of importing load from a CFD simulation into a FIA simulation and then performing a FIA analysis on the problem.

Therefore, we will first run ANSYS Fluent and create our mesh with the Watertight Geometry workflow (see figure 3.6) where we will be:

1. Creating a surface mesh
2. Capping the tops and bottom of the model to extract fluid regions.
3. Creating Solid/Liquid domains
4. Creating a volume mesh (polyhedral meshing)

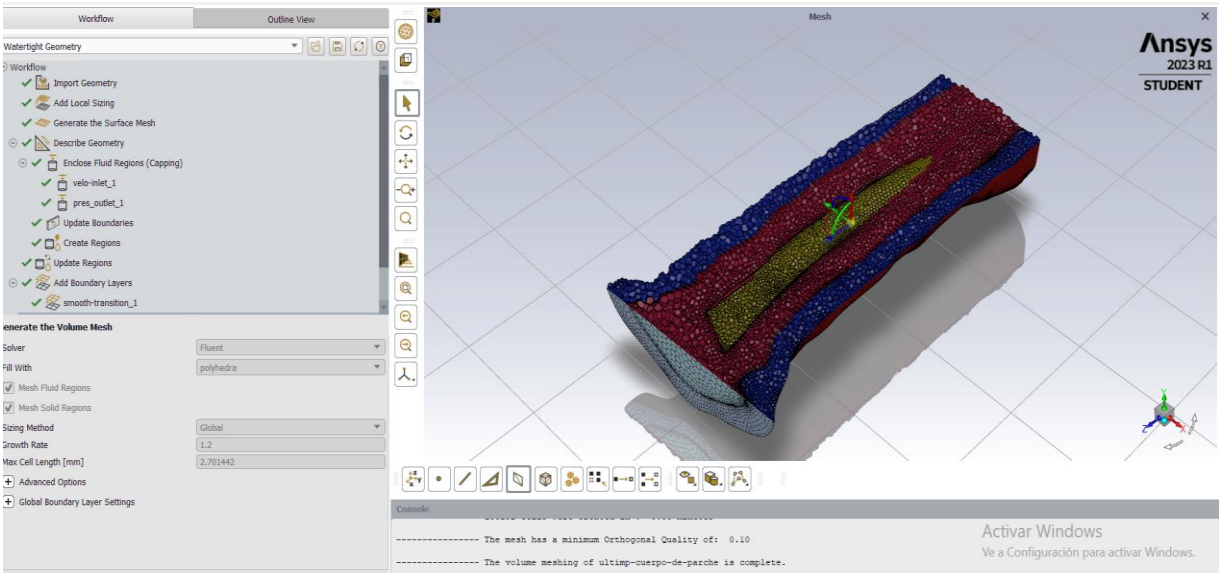

Figure 3.6: Polyhedral mesh on Watertight Geometry workflow, Ansys Fluent

INLET	Velocity-inlet
OUTLET	Pressure-outlet
DURAMATER	WALL
SPINALCORD	WALL-INTERNAL

Table 3.2: Boundary conditions

Once that has been done, we move onto the set up.

CSF is a Newtonian fluid with a density and kinematic viscosity similar to water, so we will model it as such. In order to represent the physical system accurately as it was previously justified, the flow of CSF is implemented with a periodic flow.

The solution was run as a transient with the prescribed time-varying inlet flow and CSF flow was assumed to be laminar as the Reynolds number throughout the flow domain is overall inferior to 2300 (Martin et al., 2013).

As it was previously stated, CSF behaves like a Newtonian viscous fluid, which means that in a shearing flow, the shear stress will be proportional to the strain rate (Lever, 2005b). Therefore, the pulsatile flow of the cerebrospinal fluid in the SAS is described by Navier–Stokes equations. As it is a Newtonian fluid with a laminar flow in a non-porous domain, they can be simplified as follows (Kundu, Cohen & Dowling, 2016):

Conservation of Momentum:

$$\rho\left(\frac{Du}{Dt}\right) = -\nabla p + \mu\nabla^2 u + \rho g \qquad (1)$$

Where u is the Eulerian velocity field, ρ is the density, p is the fluid pressure μ is the dynamic viscosity, t is the time, ∇ is the spatial gradient operator and ∇^2 is the Laplacian operator: in Cartesian coordinates, $\nabla=(\partial/\partial x,\partial/\partial y,\partial/\partial z)$ and $\nabla^2=\nabla\cdot\nabla=\partial^2/\partial x^2+\partial^2/\partial y^2+\partial^2/\partial z^2$

And where $\frac{Du}{Dt} = \frac{\partial u}{\partial t} + u \cdot \nabla u$ which represents the material derivative.

Besides, we have the continuity equation expressing conservation of mass for an incompressible fluid:

$$\nabla\cdot u=0 \qquad (2)$$

The simplification of the Navier-Strokes equations is based on several assumptions (Kundu, Cohen & Dowling, 2016):

1. Newtonian fluid: This assumption means that the fluid obeys Newton's law of viscosity, which states that the shear stress in a fluid is proportional to the rate of deformation. This simplifies the viscosity term in the momentum equation to be linearly proportional to the rate of deformation tensor, which is the symmetric part of the velocity gradient tensor.

2. Laminar flow: This assumption means that the fluid flows in parallel layers, with little or no mixing between the layers. This simplifies the momentum equation by neglecting the convective term, which represents the non-linear advection of fluid particles by the velocity field.
3. Incompressible flow: This assumption means that the fluid density is constant throughout the domain. This simplifies the mass conservation equation to be a continuity equation, which states that the divergence of the velocity field is zero.
4. Non-porous domain: This assumption means that the domain has a solid boundary with no fluid flow across it. This simplifies the momentum equation by assuming that the fluid velocity at the boundary is zero, which is known as the no-slip condition which can be represented using a vector notation as:

$$\begin{pmatrix} u_1 \\ u_2 \\ u_3 \end{pmatrix} = \begin{pmatrix} 0 \\ 0 \\ 0 \end{pmatrix}$$

The Navier-Stokes equations were discretized in space with a second-order upwind scheme and in time with a second-order implicit scheme, and Pressure-Velocity Coupling was selected as SIMPLE.

A linear distribution for the static gauge pressure of 50 Pa.

A velocity profile is prescribed on the inlet boundary of the fluid domain following a User-Defined Function (UDF).

Our UDF (see figure 3.7) defines a pulsatile sinusoidal velocity profile for CSF flow in a 3D model. The velocity varies between a maximum velocity of 0.025 m/s and a minimum velocity of 0.002 m/s (Alperin et al., 2000) over a period of 1.25 seconds (0.8 Hz). In some studies, researchers have reported a “cardiac” frequency band of 0.65 to 1.65 seconds (Chen et al., 2015). Therefore, a period of 1.25 seconds was chosen because it gives a reasonable and visually distinguishable oscillation of the flow velocity between the minimum and maximum values so we can visualize and analyze the behavior of the fluid flow over time.

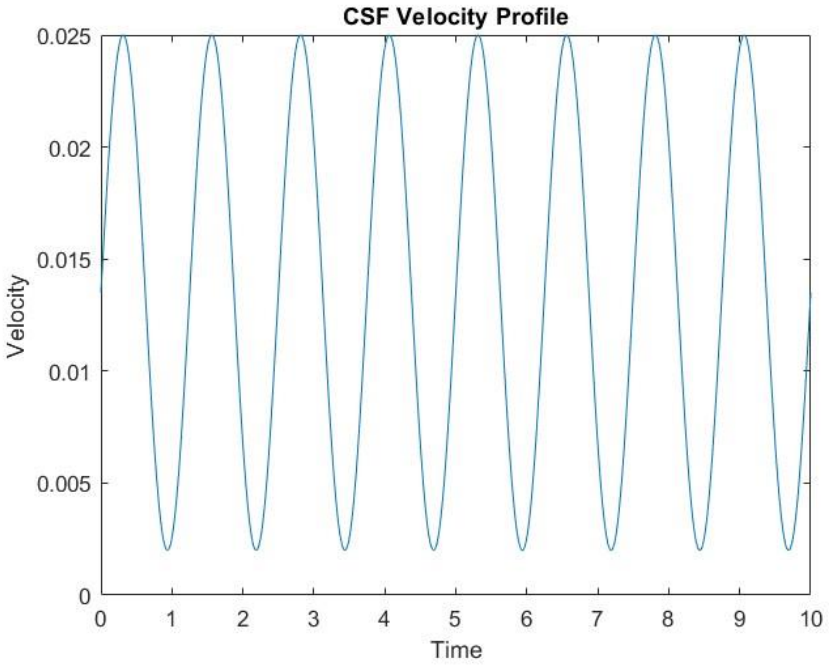

Figure 3.7: Sinusoidal Velocity Profile for Cerebrospinal Fluid (CSF) in Flow Simulation

	Spinal Cord	Duramater (SAS)	CSF
Density (kg/m^3)	1500	1130	1000
Viscosity (Ns/m^2)	-	-	0.001003

Table 3.3 (A Poroelastic Model of Spinal Cord Cavities, n.d.): Material properties

Boundary conditions	Value
Velocity-inlet	UDF function
Pressure outlet	50 Pa

Table 3.4 (Liu et al., 2017): Boundary conditions on Ansys Fluent

3.5.2 Transient Structural Module

Now that the force data has been calculated, it can be transferred onto the transient structural analysis module on ANSYS.

For a CSF flow simulation with the spinal cord, we chose a transient analysis because the flow of CSF is dynamic and changes with time. Transient analysis will allow us to track the changes in the flow over time and provide a more accurate representation. The general governing equation for a transient analysis is (*15.2. Transient Analysis*, 2017):

$$[M]\{\ddot{u}(t)\} + [C]\{\dot{u}(t)\} + \{F^i u(t)\} = \{F^a(t)\} \qquad (3)$$

Where $[M] = structural\ mass\ matrix, [C] = structural\ damping\ matrix, \ddot{u}(t) = nodal\ acceleration\ vector, \dot{u}(t) = nodal\ velocity\ vector$, u(t)=nodal displacement vector, $F^i u(t) = internal\ load\ vector\ and\ F^a(t) = applied\ load\ vector.$

This analysis produces time-dependent results as it considers the time derivative of displacement, which includes velocity and acceleration. The computation of the system response considers both inertia and damping.

The deformation and shear strain of the spinal cord are determined here. In order to do that, the software uses a finite element method and preconditioned conjugate gradient solver.

Both the spinal cord and the SAS are represented as isotropic materials and their materials properties were obtained from literature:

	Spinal Cord	Duramater (SAS)
Density (kg/m^3)	1500 kg/m^3	1130 kg/m^3
Young Modulus [Pa]	5000 Pa	3.15 10^7 Pa
Poisson ratio	0.4	0.45

Table 3.5 (A Poroelastic Model of Spinal Cord Cavities, n.d.): Bulk system material properties

We will not be differentiating between grey and white matter when modelling the spinal cord because even though they do have different properties, the differentiation between the two of them has been found to only have little influence on regions that depend on the anatomy of a person (Stverud et al, 2015)

Furthermore, we will be using two fixed supports on our spinal cord and duramater on both the top and bottom base as they provide better stability and prevent unnecessary deformations or rotations in the model. The decision was made was based on the fact that The spinal cord is anchored distally by the filum terminale (Adigun, 2022). If only one fixed support is applied, it will constrain the movement of the spinal cord in only one direction, either in the axial or in the transverse direction. This would not accurately represent the behaviour of the spinal cord. By applying two fixed supports, the movement of the spinal cord in both directions can be constrained, resulting in a more accurate and stable simulation (see figure 3.8). In addition to that we also used the coupled system in FSI simulations because it allows us to model the interaction between the fluid and solid regions in a way that considers the effects of both on each other.

We chose a time step of 0.01s and end time of 10s because smaller time step results in more accurate results even though it requires more computational resources and therefore increases the simulation time. Similarly, an end time of 10 s is chosen based on the length of the simulation required to capture the relevant flow dynamics and ensure that the system has reached a steady state.

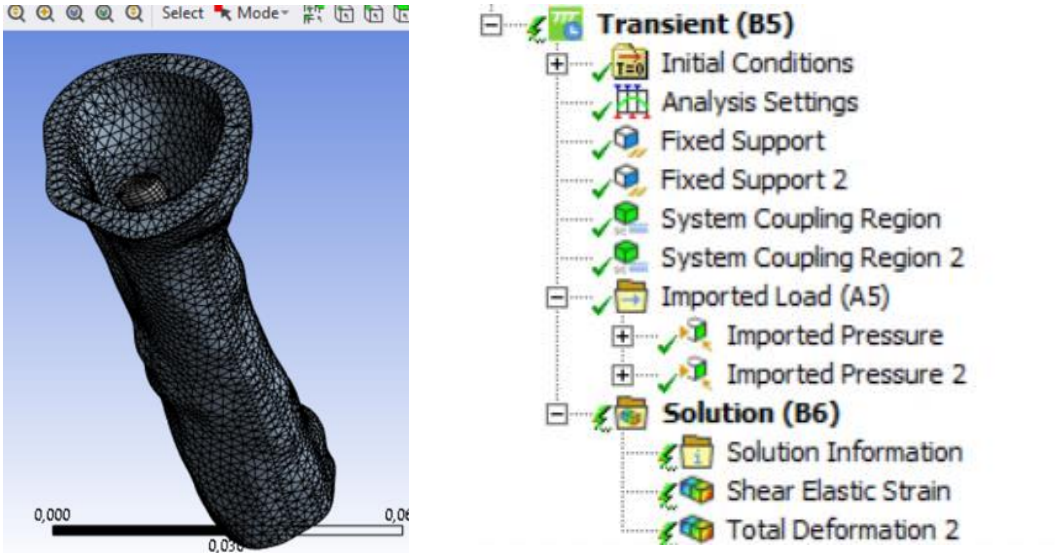

Figure 3.8: Graphical representation of the mesh and boundary conditions on Transient Structure Module

3.6 Updates for Central Canal and Syrinx Incorporation

3.6.1 Modelling the Central Canal

To begin with, we used the model that we had previously developed by segmenting an MRI (as it was carefully explain in chapters 3.1 to 3.5). We then used *Spaceclaim* software to add a small cylinder of the same length as the spinal cord, with a diameter of 1.5 mm (see figure 3.9). This tube represents the central canal of the spinal cord.

One of the reasons why we had to add the central canal manually was that its size. It is so small that it is often not visible on MRIs or difficult to segment accurately.

After adding the central canal (see figure 3.10), we had to assign material properties to it. In this case, we assumed the same values for the central canal as those used for the spinal cord. These values were taken from the literature that was previously stated.

It is worth noting that the addition of the central canal is an important step forward in simulating the behaviour of the spinal cord and cerebrospinal fluid as it is more accurate.

The mesh was once again created with the Watertight Geometry workflow on Ansys Fluent (see figures 3.11, 3.12 and 3.14)

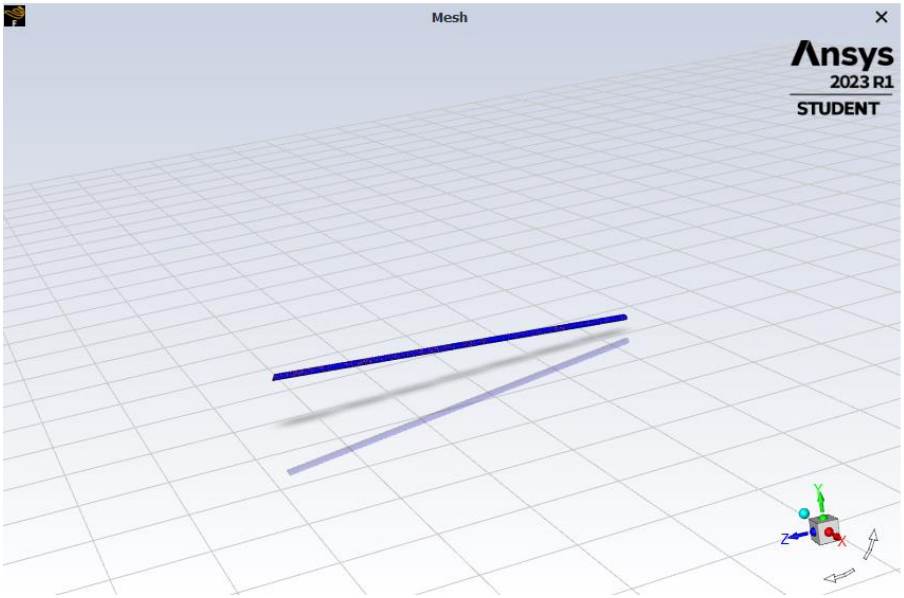

Figure 3.9: Image of the small cylindrical structure representing the central canal

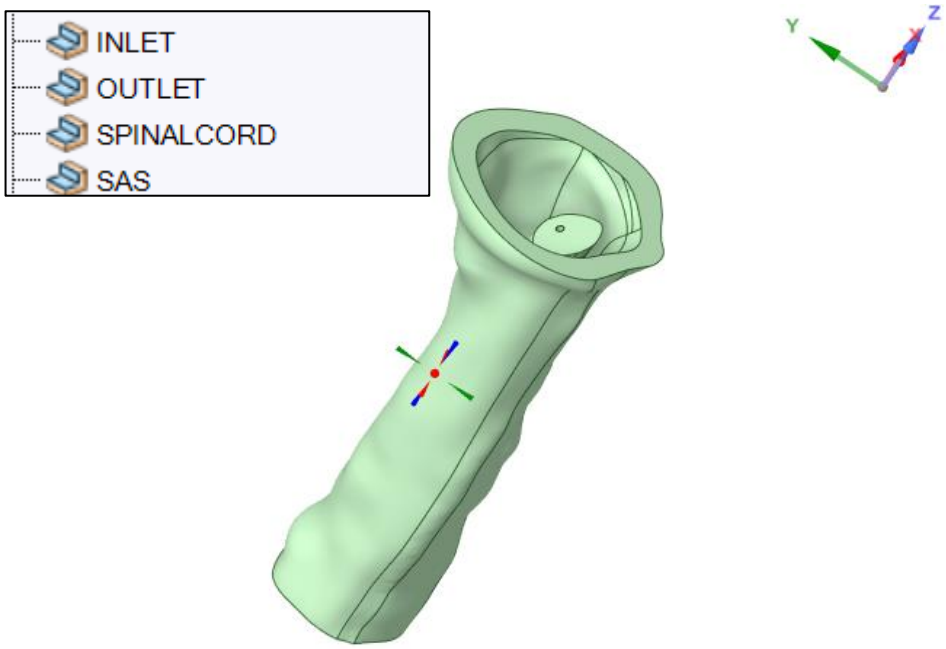

Figure 3.10: Three-dimensional model of cerebrospinal fluid space, spinal cord, and central canal

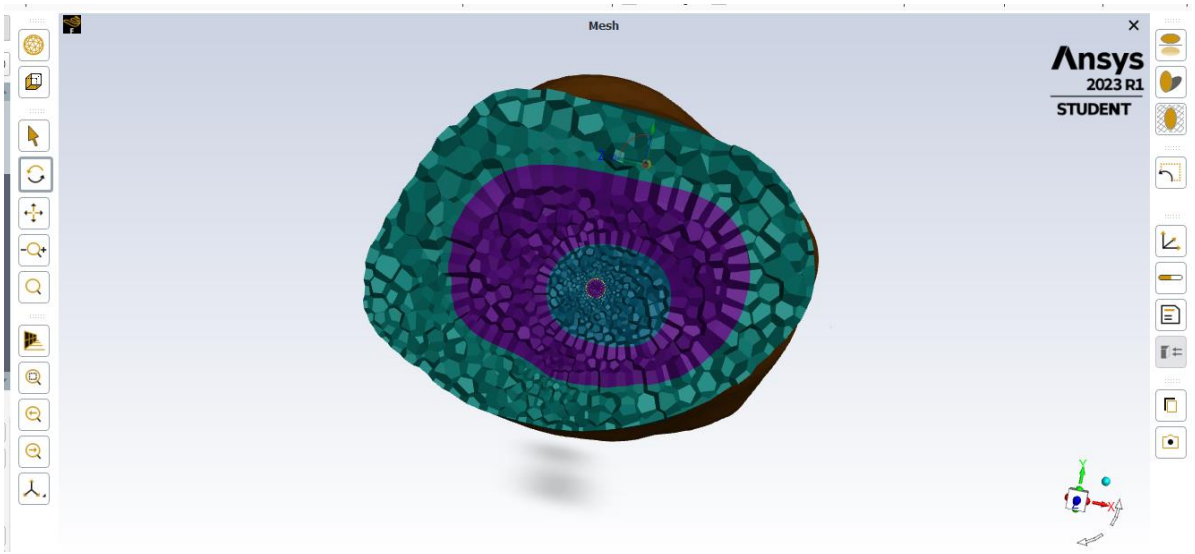

Figure 3.11: Mesh Visualization of CSF Space, Spinal Cord, and Central Canal Model with Z-Axis Cut

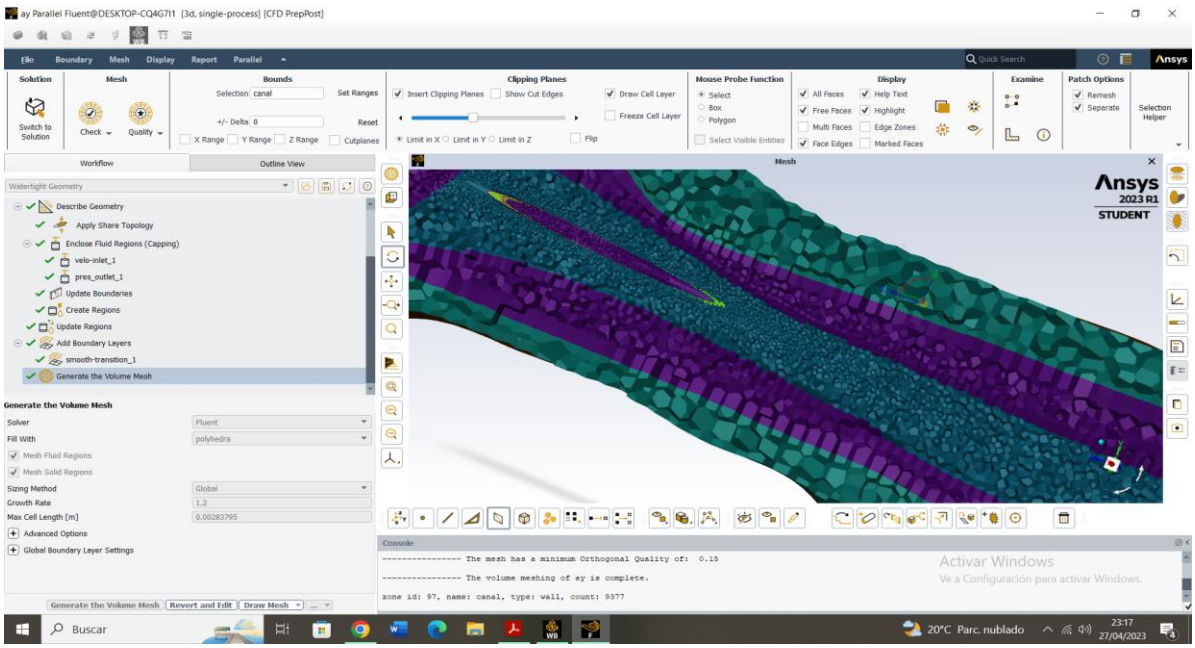

Figure 3.12: Mesh Visualization of CSF Space, Spinal Cord, and Central Canal Model with X-Axis Cut

3.6.2 Modelling the syrinx

After segmenting the MRI to create the initial model of the CSF space and spinal cord, we faced the challenge of including the syrinx in the model due to its small size. Given the resolution limitations of the MRI, we decided to manually add a small object to represent the syrinx within the central canal using *Spaceclaim* software.

The object was designed to have the same dimensions as the syrinx and placed inside the central canal (see figure 3.13). The syrinx as a solid object, therefore we must define contact regions between the syrinx and the walls of the central canal. This will ensure that contact forces are properly transmitted between the two surfaces.

It's important to note that because the syrinx is touching the walls of the central canal, it may be causing deformation or other effects that influence the behaviour of the system.

To ensure accuracy in the simulation, we used the same density value for the syrinx material as we did for the cerebrospinal fluid. The rest of values were acquired from literature:

	Syrinx
Density (kg/m^3)	1000 kg/m^3
Young Modulus [Pa]	2000 Pa
Poisson ratio	0.25

Table 3.6 (Martin et al., 2005), (Rusbridge et al., 2006): Mechanical Properties of Syrinx Cavities

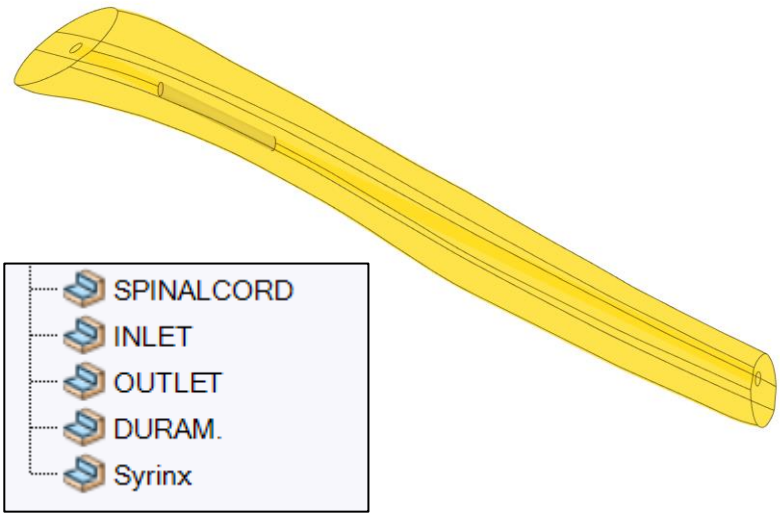

Figure 3.13: Visualization of syrinx within the spinal cord

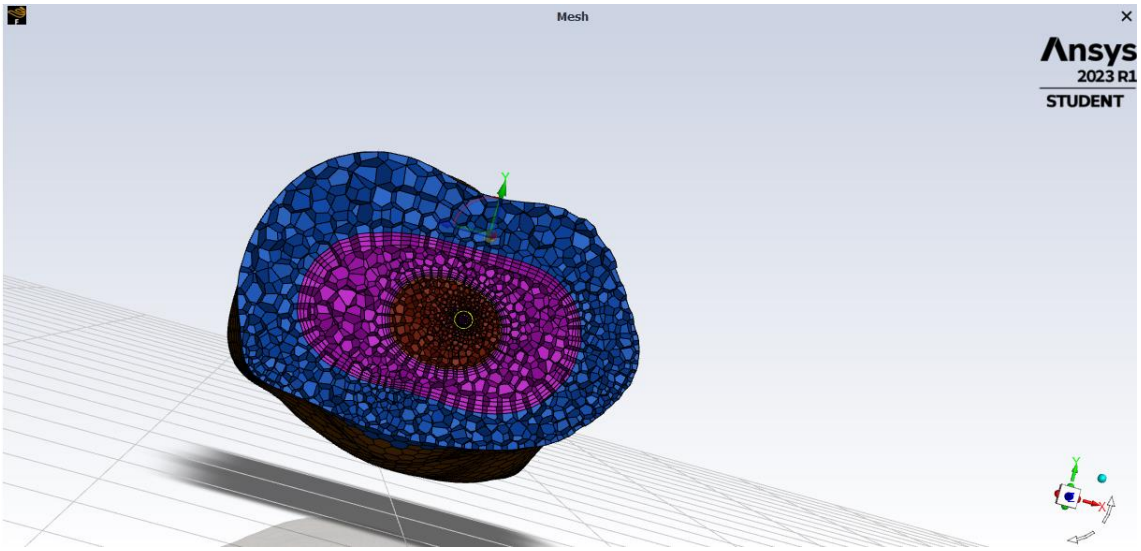

Figure 3.14: 3D Mesh Model of Spinal Cord with Syrinx Inside Central Canal and cut in Z-Axis

4

Results

The results of the ANSYS simulations completed for this study are included in this chapter. The use of simulations in this dissertation was necessary because they provide a low-cost and easily accessible environment that allows a better understanding of the behaviour of physiological processes.

4.1 Weightless conditions

In this case, we simulate weightless conditions. When we add weightless conditions to our structural transient analysis, the analysis assumes that the structure is not affected by gravitational forces. This can result in a change in the deformation results because the analysis is considering only the external loads and boundary conditions, meaning that the structural response of the system is mainly driven by the forces and loads applied to it, rather than the influence of gravity

4.1.1 CSF-Spinal Cord Model

Our first model simulates the cerebrospinal fluid (CSF) flow and the spinal cord with the aim of trying to understand the factors that lead to syrinx formation and therefore syringomyelia.

This section shows the effects of spinal cord deformation due to pressure gradients and analyses the effects CSF flow in our model.

4.1.1.1 Pressure

The pressure wave in the caudal direction in our model resulted in pressure gradients on our domain. Figure 4.1 displays the pressure gradient along the model.

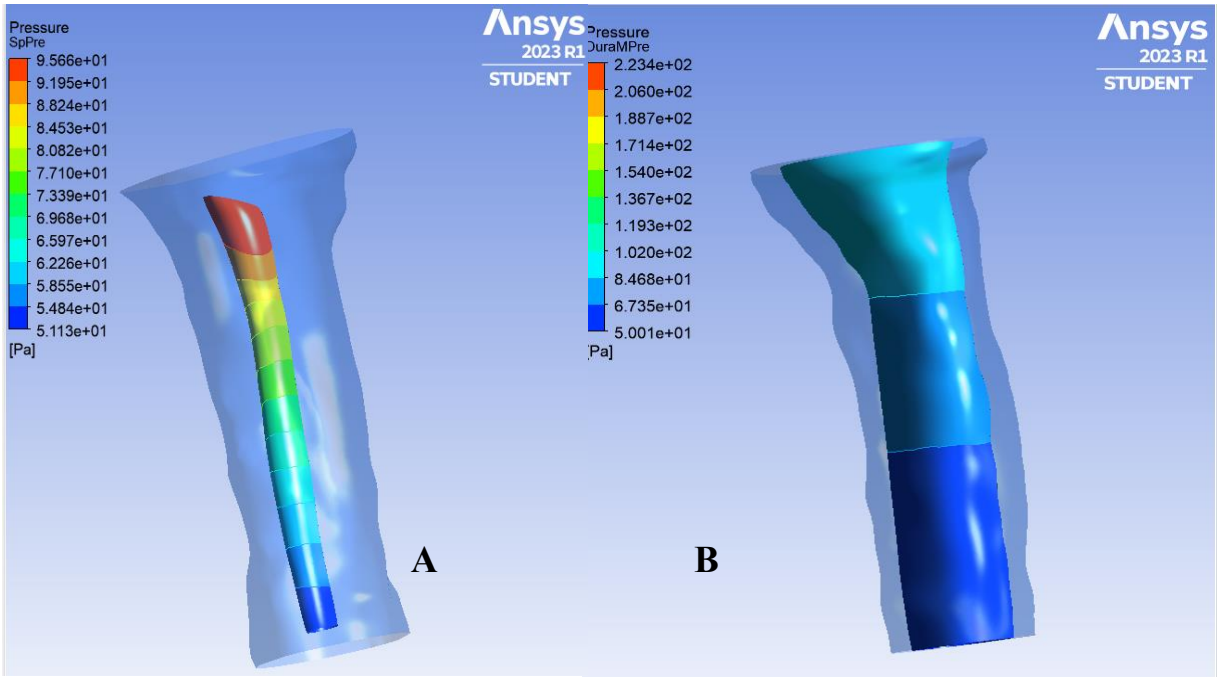

Figure 4.1: Pressure gradients [Pa]: (A) Spinal cord (B) Duramater

For (A): The pressure distribution is likely a result of the fluid flow interacting with the walls of the spinal cord. It shows a pressure drop along the length of the spinal cord. This pressure drop can be attributed to the flow behavior and geometry. As the cerebrospinal fluid (CSF) flows through the SAS (spinal subarachnoid space) surrounding the spinal cord, it experiences resistance and friction due to the narrow passages and interaction with the spinal cord surface. This resistance causes a decrease in pressure along the flow path.

For (B): The pressure gradient shows a decreasing pressure gradient along the dura mater surface. The dura mater (the outermost layer surrounding the spinal cord and subarachnoid space), experiences the effects of the CSF flow. As the CSF flows along the dura mater, it imparts pressure on the surface, creating a pressure distribution.

4.1.1.2 Velocity Vectors

Velocity Vectors of the CSF are shown below in figure 4.2

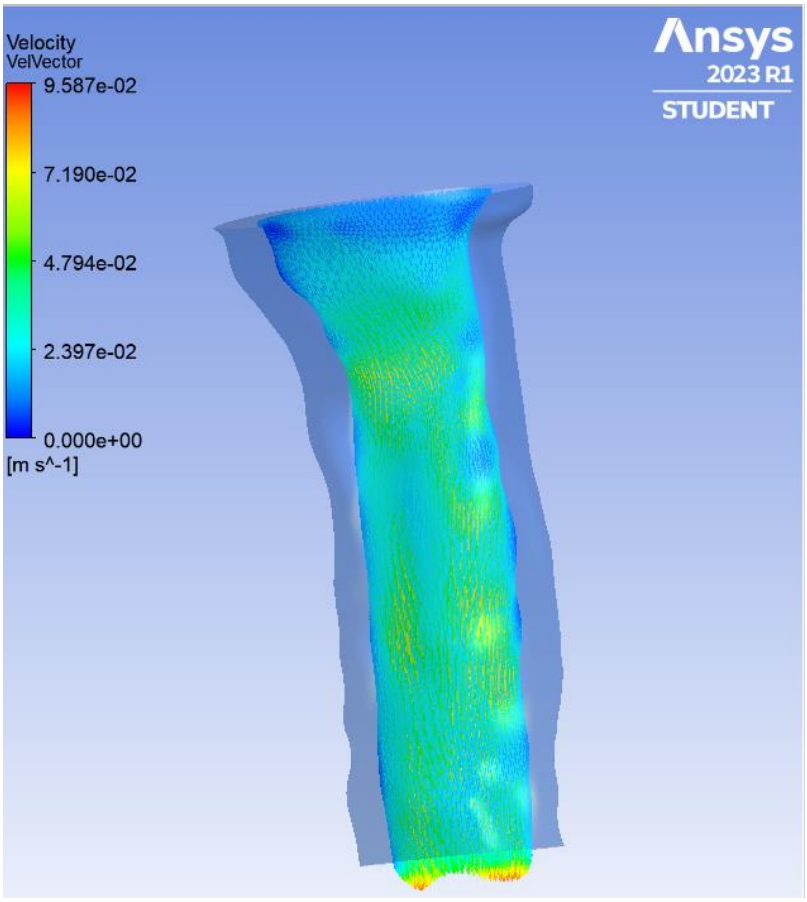

Figure 4.2: Velocity vector plot of the CSF coloured by velocity magnitude.

In this plot (see figure 4.3), each velocity vector is represented by an arrow, and its length and orientation indicate the magnitude and direction of the fluid velocity at that point. Areas with high velocity are be represented by longer, more intense arrows and a warmer colour, while areas with lower velocity are represented by shorter, less intense arrows and a cooler colour.

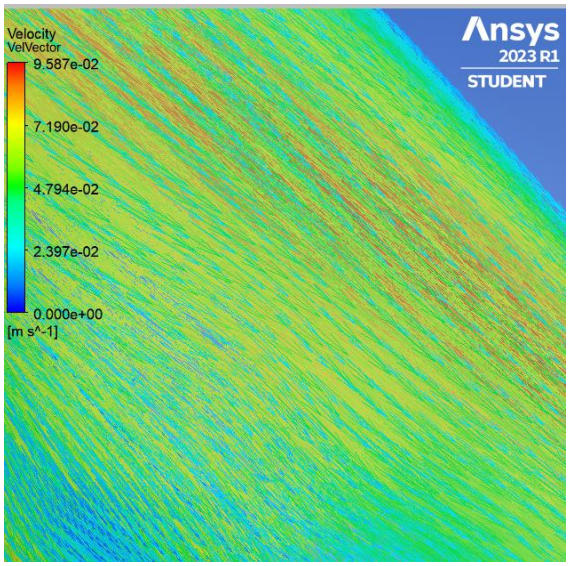

Figure 4.3: Zoom of the velocity arrows.

The arrows near the edges of the plot represent the fluid that is in contact with the walls of the spinal cord or other structures. This plot provides insight into the overall flow pattern and velocity distribution of the CSF within the CSF space.

4.1.1.3 Streamlines

Figure 4.4 illustrates the pathlines depicting the flow of CSF through the CSF space. The streamlines begin with low velocity, gradually increase in velocity, and reach maximum velocity at the midpoint. After that, the velocity decreases again towards the end. This velocity profile follows a parabolic pattern commonly observed in laminar flows, where the pressure gradient drives the flow due to CSF production and absorption.

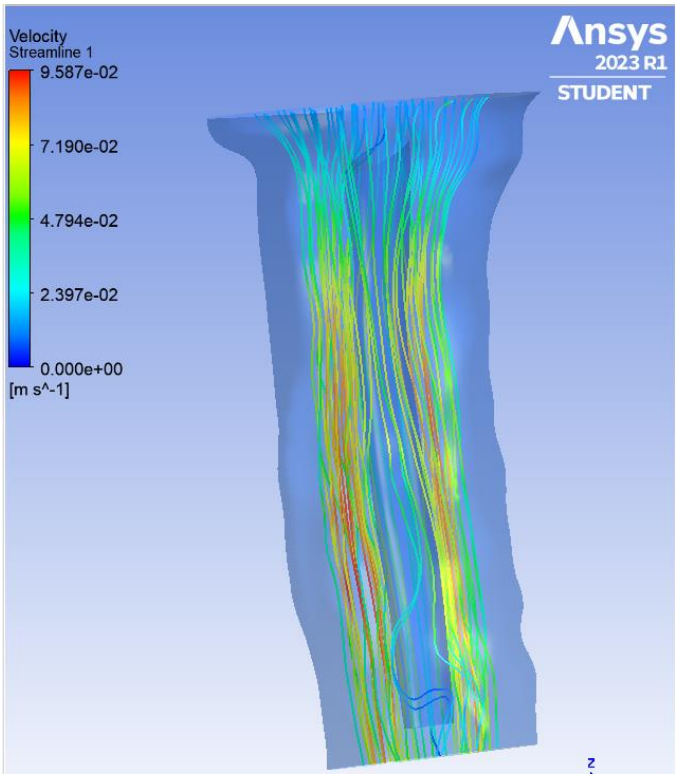

Figure 4.4: Streamlines coloured by velocity of the CSF

4.1.1.4 Wall Shear Stress

The wall shear stress contour on picture 4.5 shows the distribution of shear stress along the surface of both the CSF space and the spinal cord. The dura mater can experience shear stresses as the fluid flows past it. A low magnitude of shear stress on the dura mater tissue could suggest a relatively low level of deformation or stretching of the tissue due to the flow of CSF.

Low shear stress regions on the dura mater could suggest areas where the CSF flow is relatively smooth and steady.

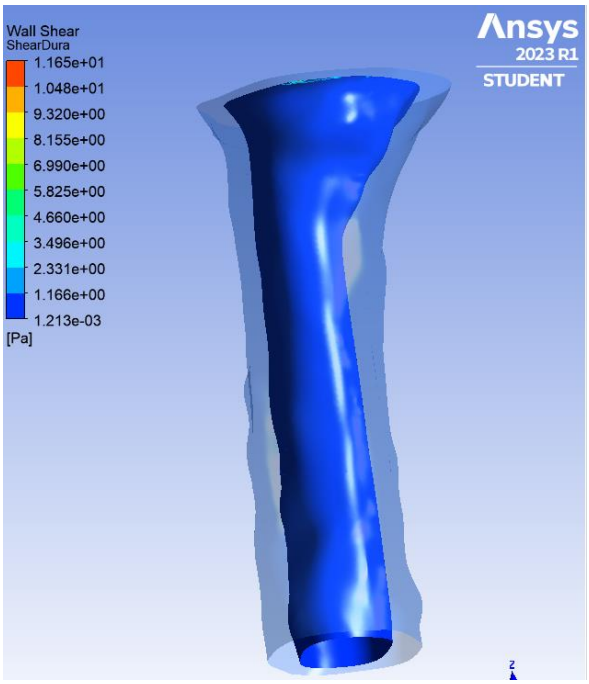

Figure 4.5: Shear stress contour on the dura mater tissue

The visualization of shear stress reveals predominantly moderate to high levels along the entire length of the spinal cord (see figure 4.6). Higher stress flow could potentially contribute to the development or progression of syringomyelia by affecting the biomechanical properties of the spinal cord tissues.

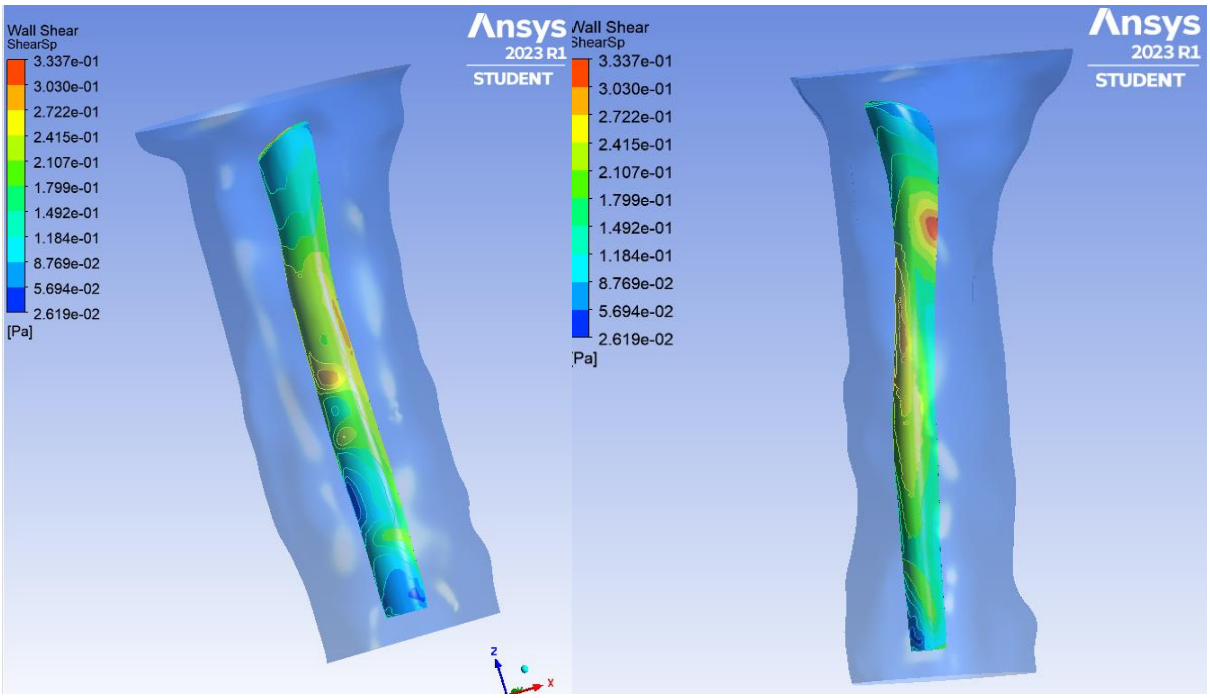

Figure 4.6: Wall Shear stress contour of the spinal cord

4.1.1.5 Deformation

The deformation (see figure 4.7) indicates that the mid-section of the spinal cord is experiencing relatively higher mechanical stress compared to other regions. This stress can potentially impact the structural integrity of the spinal cord tissue, leading to tissue damage or compression. This can result in compression or displacement of neural structures, including nerve fibers and blood vessels, affecting the functionality and communication of these structures, leading to neurological symptoms or impairments.

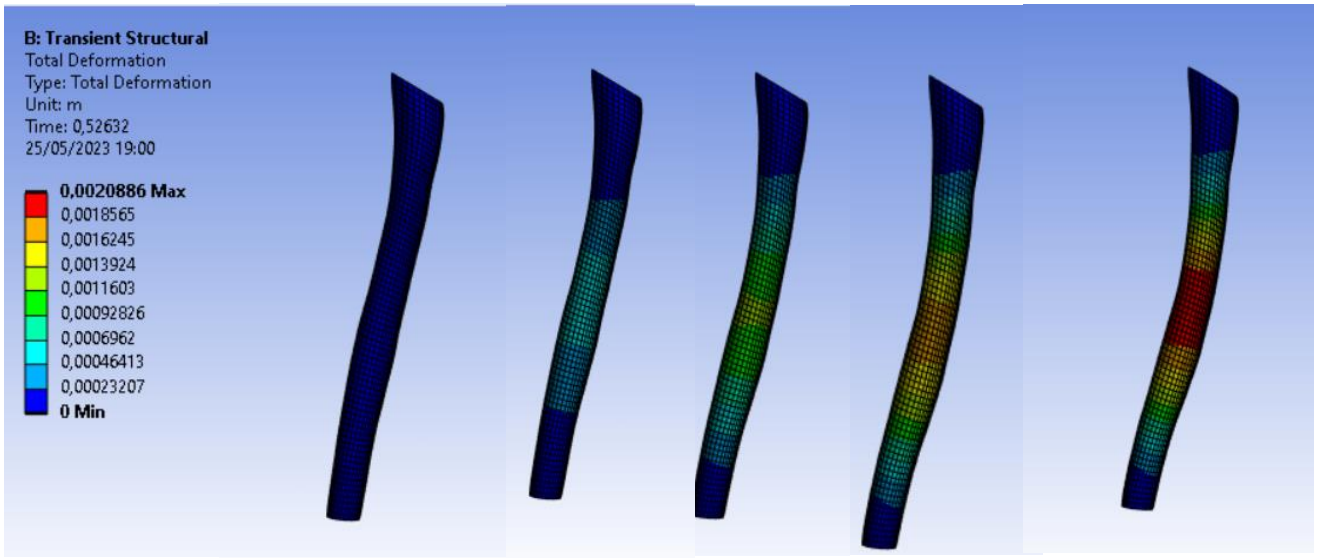

Figure 4.7: Structural Deformation of the Spinal Cord in Response to Pressure Gradient Changes in Cerebrospinal Fluid Flow under weightless conditions

4.1.1.6 Shear Stress Deformation

This concentration of shear strain (see image 4.8) suggests that the bottom middle region is subjected to increased shearing forces. In relation to syringomyelia, the elevated shear strain in the bottom middle region may contribute to the development or progression of the condition. The shear deformation can disrupt the normal tissue architecture and cellular integrity, potentially leading to the formation of fluid-filled cavities within the spinal cord.

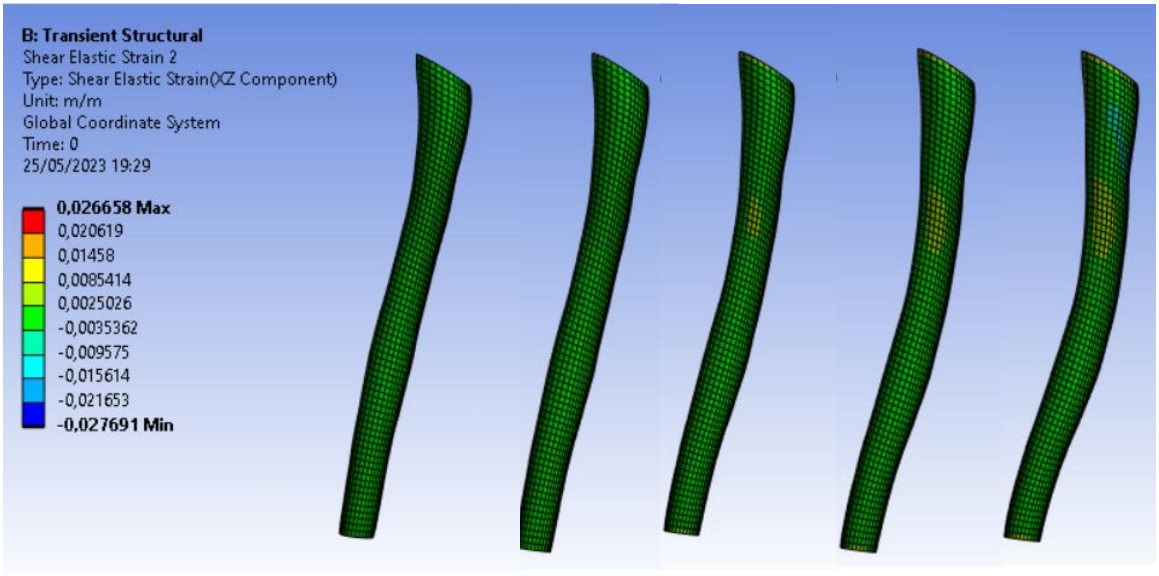

Figure 4.8: Visualization of Shear Stress Contours and Deformations in a Spinal Model

4.1.2 CSF-Spinal Cord-Central Canal Model

We have developed an updated version that includes the central canal of the spinal cord. This model builds on our previous work. With this update we aim to improve the accuracy of our computational model.

4.1.2.1 Pressure

When visualizing the results obtained for this model on ANSYS fluent (see image 4.9) we realized that the pressure distribution in the model is similar to the model without the central canal. This may be because the central canal is a very small compared to the model and does not have a significant effect on the flow dynamics of the system. However, the slightly higher values observed within the model are a consequence of the additional resistance that the central canal adds to the flow, even if it is small.

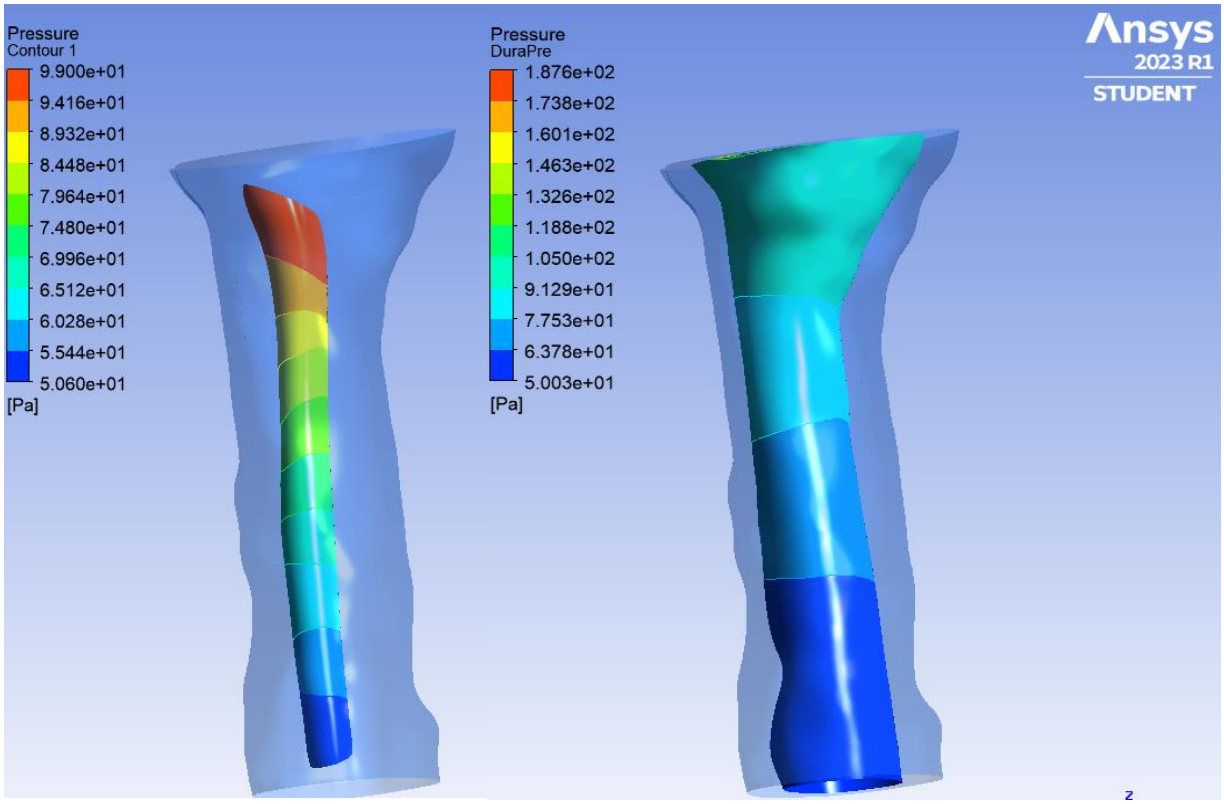

Figure 4.9: A. Image showing pressure distribution for the spinal cord. B . Image showing pressure distribution for the duramater tissue

4.1.2.2 Velocity vectors

Since the dimensions of the canal are small compared to the spinal cord's ones, the addition of the central canal does not significantly impact the fluid dynamics, when we try to visualize the results (see figure 4.10), the distribution seems to be the same but with slightly higher velocity values.

However, small changes in the geometry can have a cumulative effect on the fluid dynamics and it is important to study any changes made even if they seem insignificant.

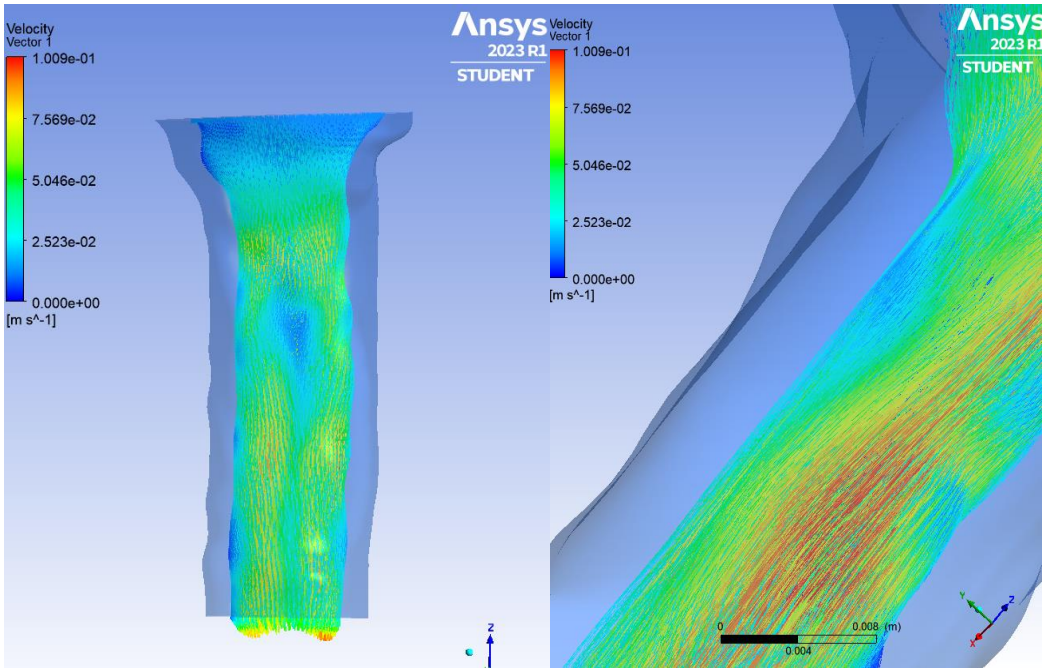

Figure 4.10: Velocity Vectors: Normal and Zoomed-In Views

4.1.2.3 Streamlines

When visualizing the pathlines (see figure 4.11), we realize once again that the velocity gradient is similar due to the fluid following a similar path. However, the model with the central canal has a slightly higher velocity due to the additional space for fluid to flow through. This is expected as the presence of the central canal allows for more room for fluid to move.

The increased recirculation at the bottom of the model in the presence of the central canal may be due to changes in the flow patterns.

As the central canal is an enclosed space within the spinal cord, fluid will naturally flow through it, resulting in the dark blue pathlines. In the central canal, the velocity is expected to be lower than in the surrounding CSF space due to the smaller diameter of the canal.

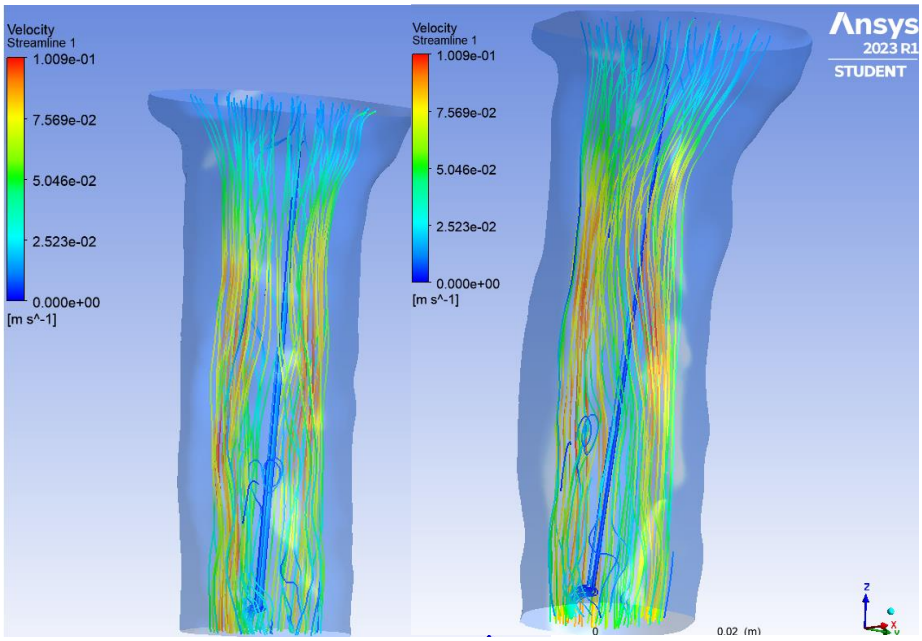

Figure 4.11: Fluid Pathlines in Spinal Cord Model with Central Canal

4.1.2.4 Wall Shear Stress

When we visualize the wall shear stress (see figure 4.12), the differences observed in wall shear values between the model with the central canal and the one without it suggest once again that the presence of the central canal influences the fluid dynamics.

The presence of higher shear stress regions could be due to changes in the flow patterns caused by the presence of the central canal.

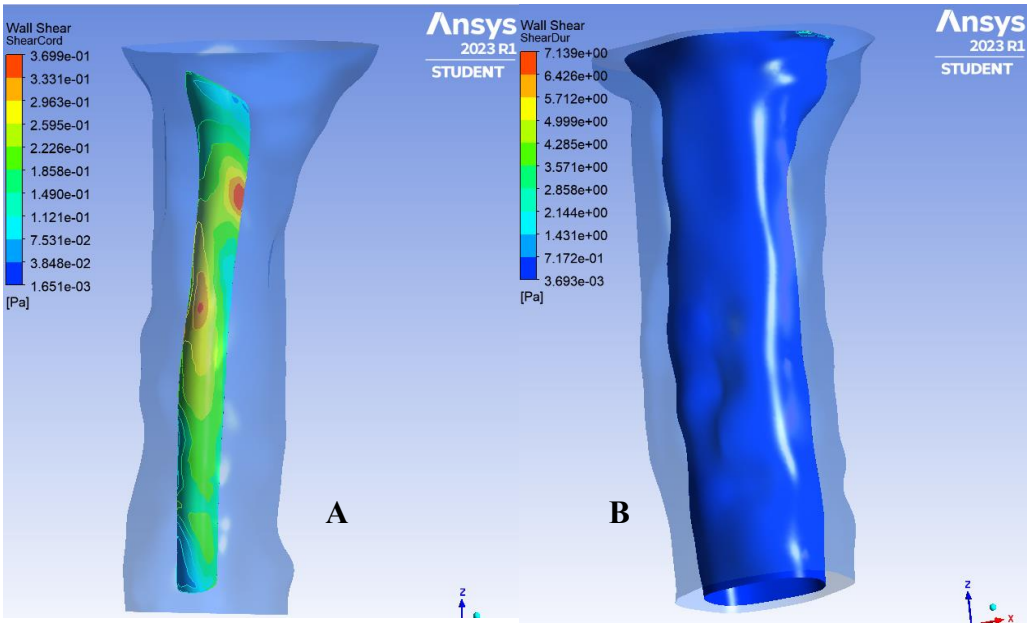

Figure 4.12: A. Wall Shear Stress Distribution in Spinal Cord Model with Central Canal. B. Wall Shear Stress Distribution in the duramater tissue

4.1.2.5 Deformation

The differences in the deformation patterns between this model the one without the central canal suggest that the central canal influences the distribution and magnitude of deformation.

In the model without the central canal, the deformation appears to be more evenly distributed, with a slightly higher concentration in the middle (due to the absence of any structural feature).

On the other hand, in the model with the central canal, the deformation is not as evenly distributed. The presence of the central canal may act as a mechanical constraint or boundary condition, causing the deformation to be more concentrated or localized in certain regions. The canal allows for some degree of fluid flow and movement within it. This fluid movement acts as a cushion, reducing the deformation of the spinal cord compared to the first model (see figure 4.13).

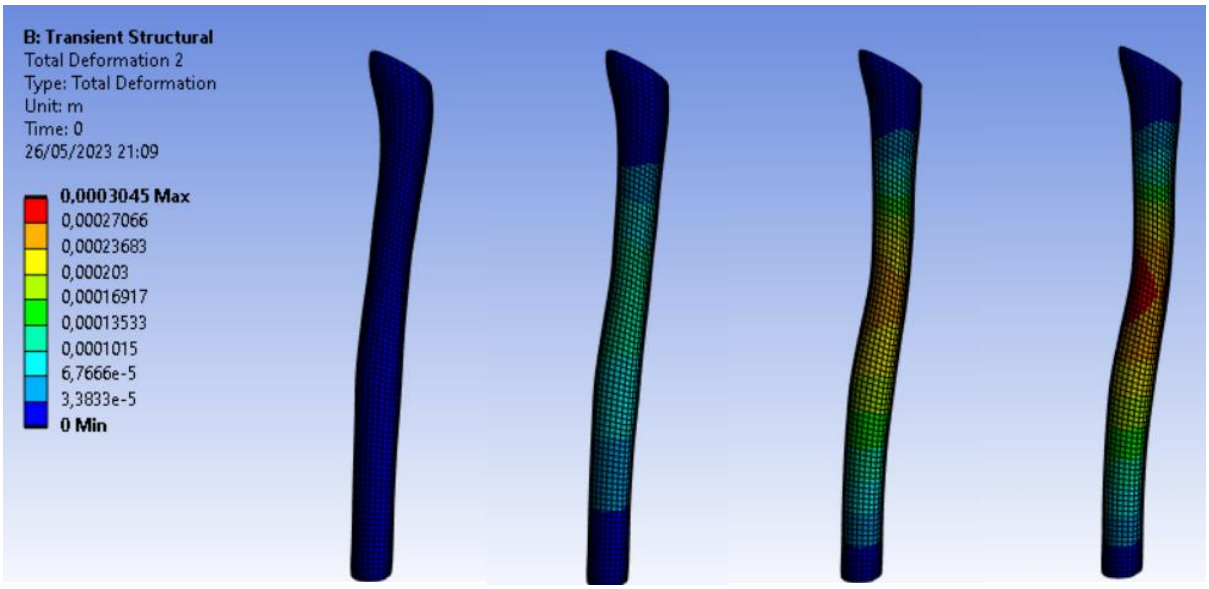

Figure 4.13:Deformation of Spinal Cord Model with Central Canal

4.1.2.6 Shear Stress Deformation

When we analyse our spinal cord model with central canal, we notice that the wall shear deformation on the XZ-axis has a once again the same distribution (see figure 4.14). However, the values are significantly higher. The presence of the central canal changes the geometry of the spinal cord model, creating a small cavity in the centre of the spinal cord where cerebrospinal fluid can flow. This cavity can alter the flow of fluid within the spinal cord, creating areas of increased or decreased flow, which can in turn affect the distribution of wall shear stress.

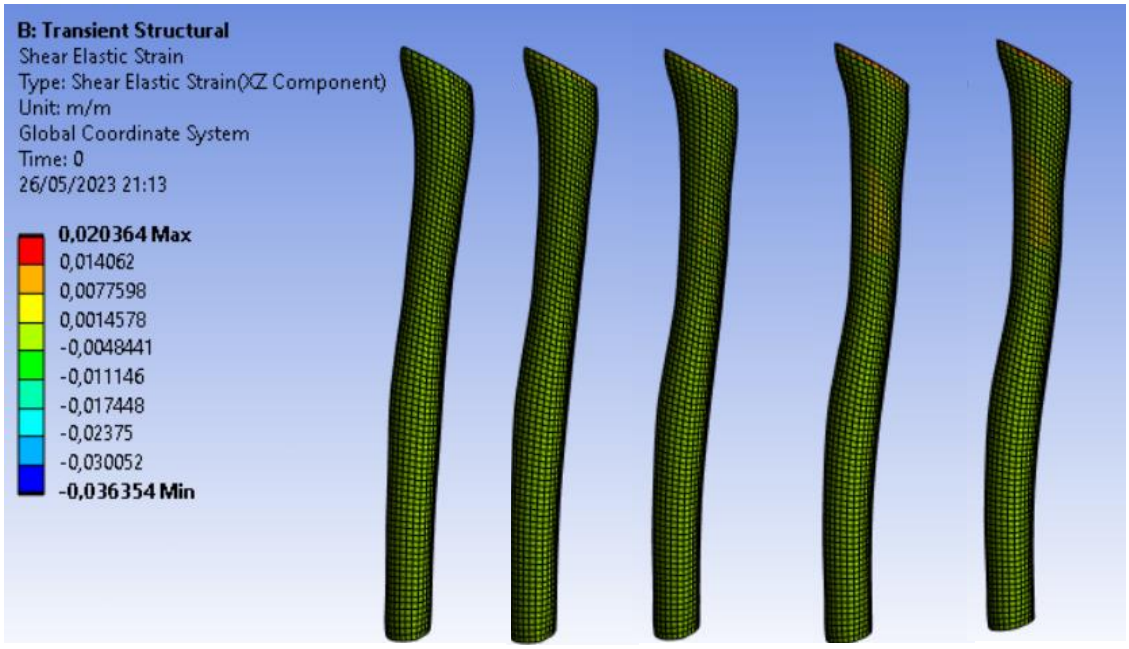

Figure 4.14: Wall Shear Deformation *on XZ-Axis in Spinal Cord Model with central canal*

4.1.3 CSF-Spinal Cord-Central Canal-Syrinx Model

To further improve the realism of our computational model, we have developed a final version that includes a syrinx within the central canal. This model also builds on our previous work.

4.1.3.1 Pressure

At first sight the pressure distribution seems to be the same as the one we obtained without the syrinx. However, there is a slight increase of the pressure values regarding of the colour distribution. The syrinx is obstructing the central canal, affecting the fluid dynamics and pressure distribution. This is because the fluid flow is now restricted by the presence of the syrinx, which can lead to an increase in pressure at certain regions (see figure 4.15).

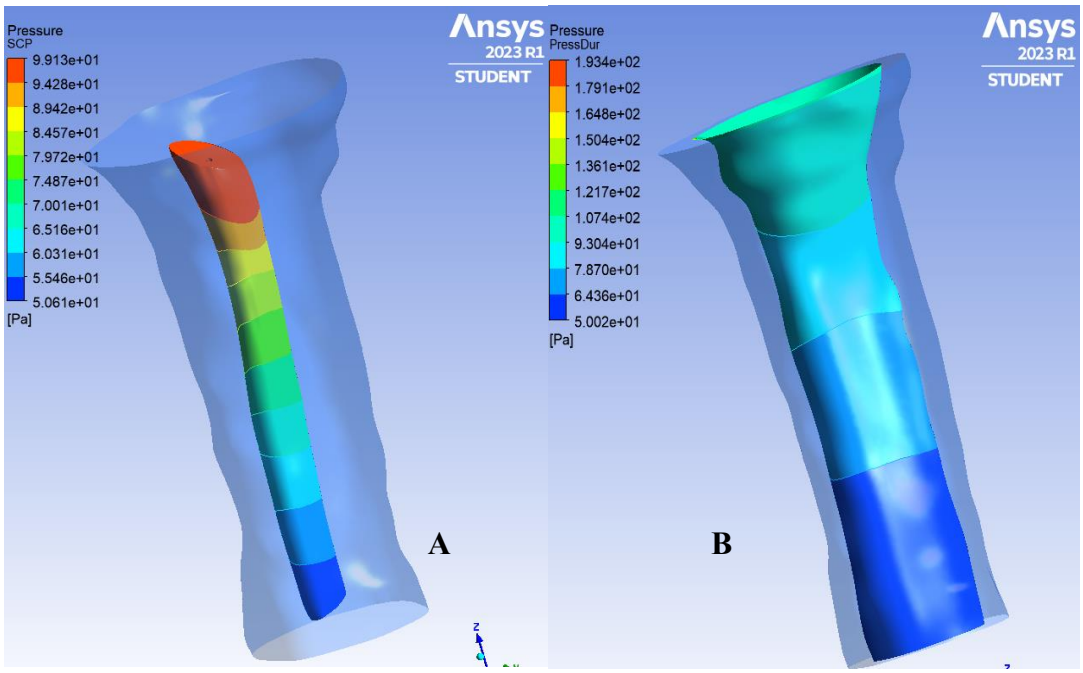

Figure 4.15: Image showing pressure distribution for the spinal cord & syrinx model. A. Spinal Cord. B. Duramater tissue

We can also analyse the syrinx's pressure gradients (see figure 4.16):

The syrinx is obstructing the central canal completely (no gaps), so the fluid flow is most likely redirected around the obstruction. That is why there are pressure gradients at the top and bottom of the syrinx and the reason why there are no pressure gradients on the body of the syrinx.

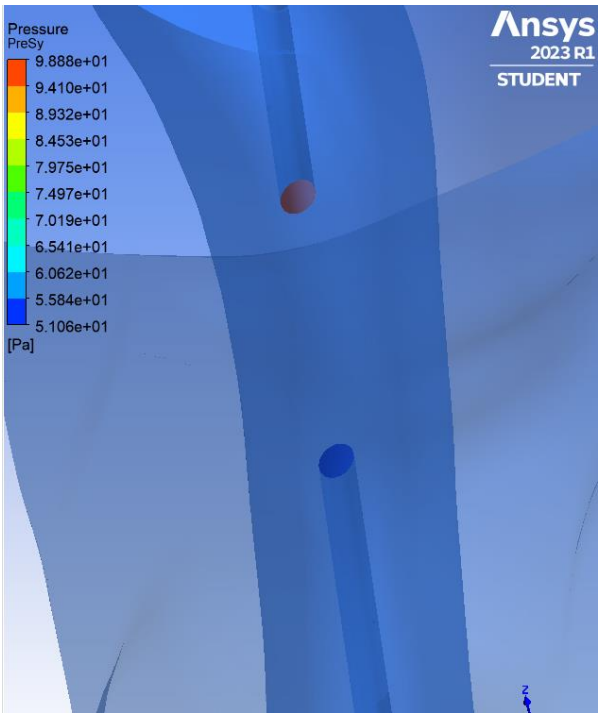

Figure 4.16: Pressure gradient distribution at top and bottom of syrinx

4.1.3.2 Velocity Vectors

The velocity vector difference between this model and the previous one was smaller than 0.0001 so they will not be discussed.

4.1.3.3 Pathlines

The presence of the syrinx inside the central canal is causing a disturbance in the flow and altering the pathlines. The syrinx acts as an obstruction. As a result, the CSF flow is disrupted, and the pathlines deviate from their typical pattern, resulting in a slight decrease in velocity (see figure 4.17).

Without the syrinx, the pathlines would normally continue along the entire length of the central canal. However, with the presence of the syrinx, the pathlines are no longer observed within the syrinx itself, indicating that the flow is being obstructed by the abnormal fluid-filled cavity.

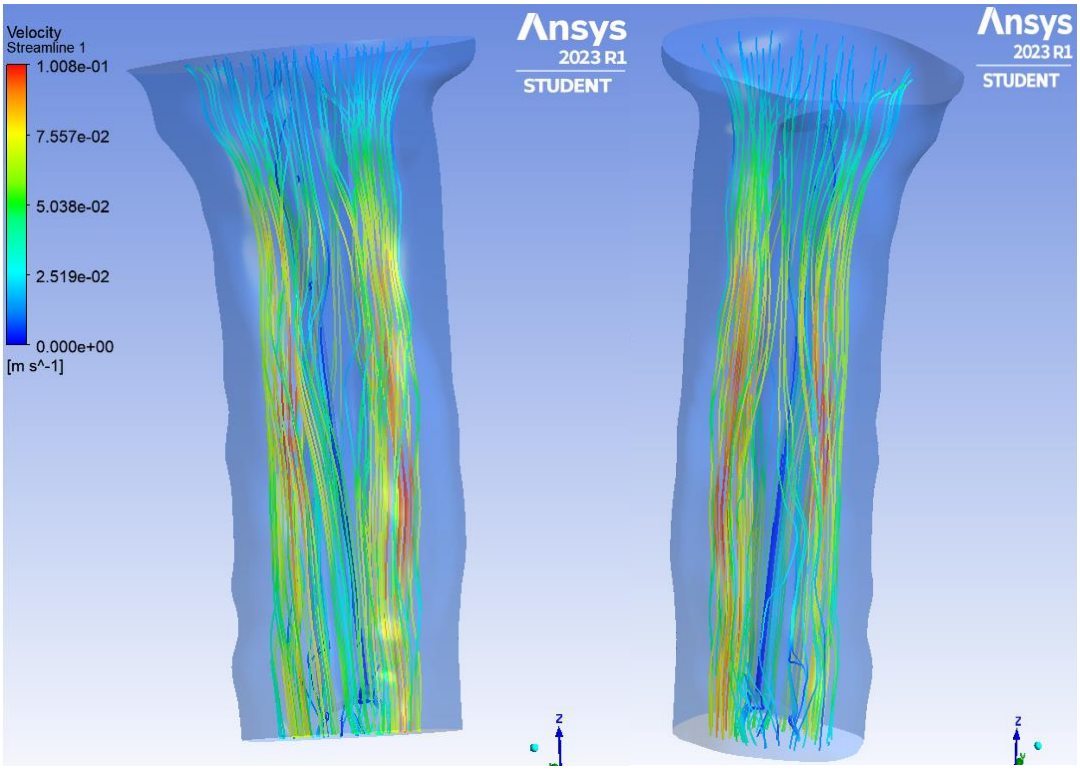

Figure 4.17: Pathlines of Flow Through Spinal Canal with Syrinx Obstruction

4.1.3.4 Wall Shear Stress

While analysing the wall shear stress on the spinal cord, we noticed that the values obtained are slightly smaller than those obtained from the model without the syrinx inside the central canal. However, the wall shear distribution remains the same. The fact that the wall shear stress values

are slightly smaller suggests that the obstruction caused by the syrinx. It is reducing the amount of force that the fluid exerts on the walls of the central canal. However, gradient distribution remains the same, indicating that the overall distribution of wall shear stress along the spinal cord is not significantly affected by the presence of the syrinx (see figure 4.18).

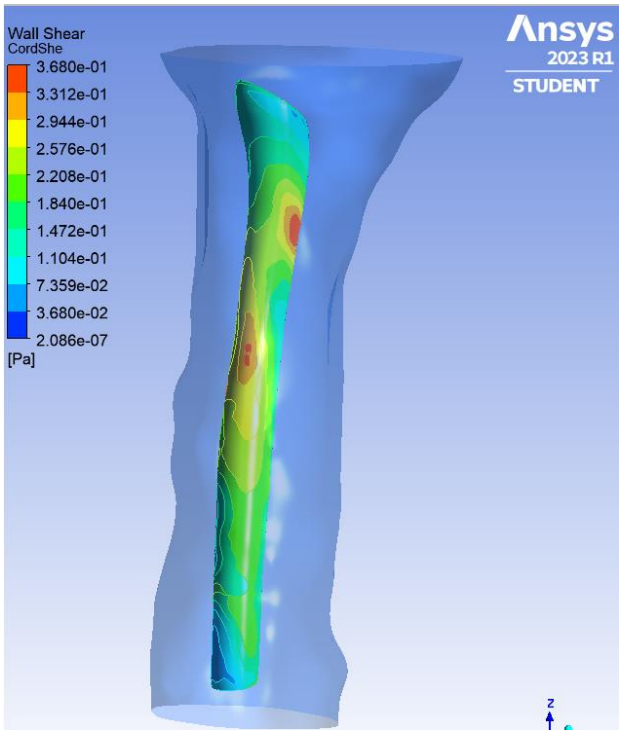

Figure 4.18: Wall Shear Stress Distribution in Spinal Cord with Syrinx Obstruction

.As the syrinx is obstructing the entire canal, the wall shear stress is only present on the top and bottom bases of the syrinx (see figure 4.19). The pattern suggests a relatively low wall shear stress at the bottom. On the other hand, the top base shows a higher shear stress. As the flow encounters the syrinx, it is forced to accelerate and change direction rapidly, creating regions of high wall shear stress.

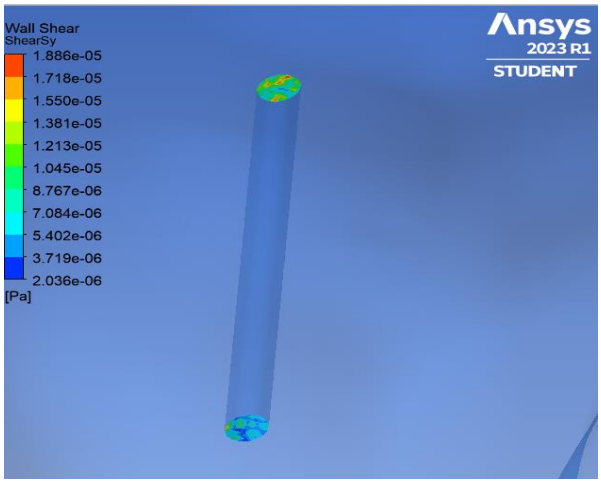

Figure 4.19: Wall Shear Stress Distribution on Syrinx Obstructing Central Canal

4.1.3.5 Deformation

We now examine the deformation of the spinal cord in our model with a syrinx inside the central canal (see figure 4.20). The deformation values are higher than those in the model without a syrinx.

When we add the syrinx inside the central canal, it creates an obstruction that alters the distribution of forces and stresses within the spinal cord, affecting the deformation. The syrinx inside the central canal acts as a fluid-filled cavity within the spinal cord, introducing additional complexities to the mechanical behaviour of the spinal cord. These complexities can result in slightly higher deformation values compared to a model without a syrinx.

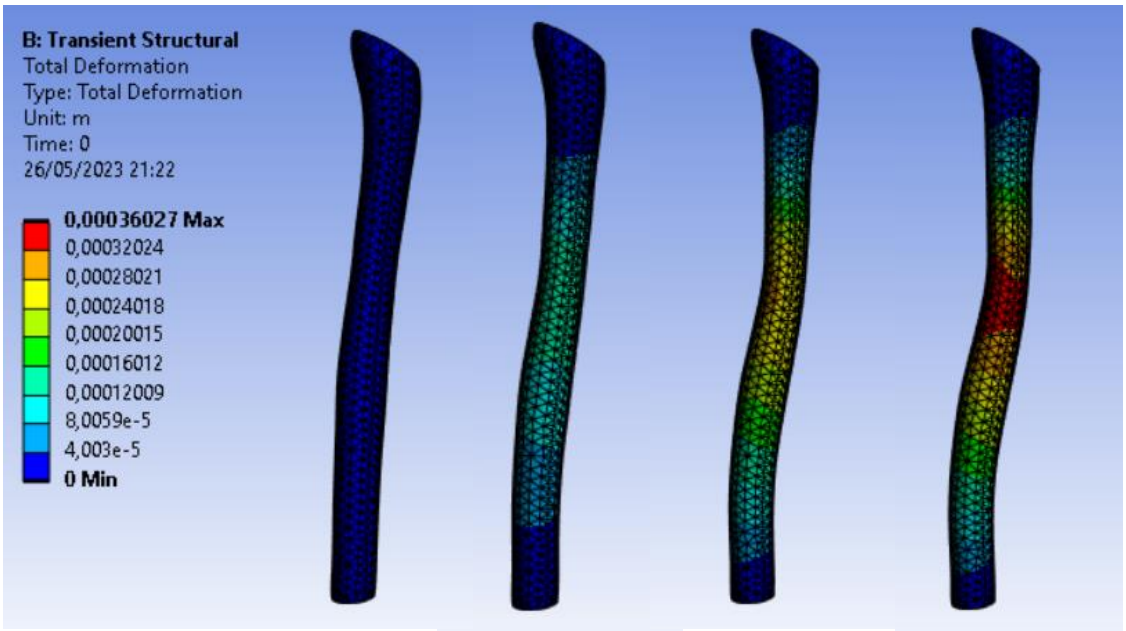

Figure 4.20: Deformation of Spinal Cord Model with Central Canal and Syrinx

When visualizing the deformation on the syrinx, we see how the syrinx deforms.

It shows that the deformation of the syrinx is not uniform as some regions are experiencing greater deformation than others (see figure 4.21). This can have implications for impact on the surrounding spinal cord tissue. Depending on the severity of the deformation, it will worsen the obstruction and compress the spinal cord more. This visualization with a gradient from high deformation at the bottom to lower deformation at the top, may give us insights into the growth of the syrinx. Regions of higher deformation may experience increased pressure and fluid accumulation, promoting further expansion and growth of the syrinx in those areas.

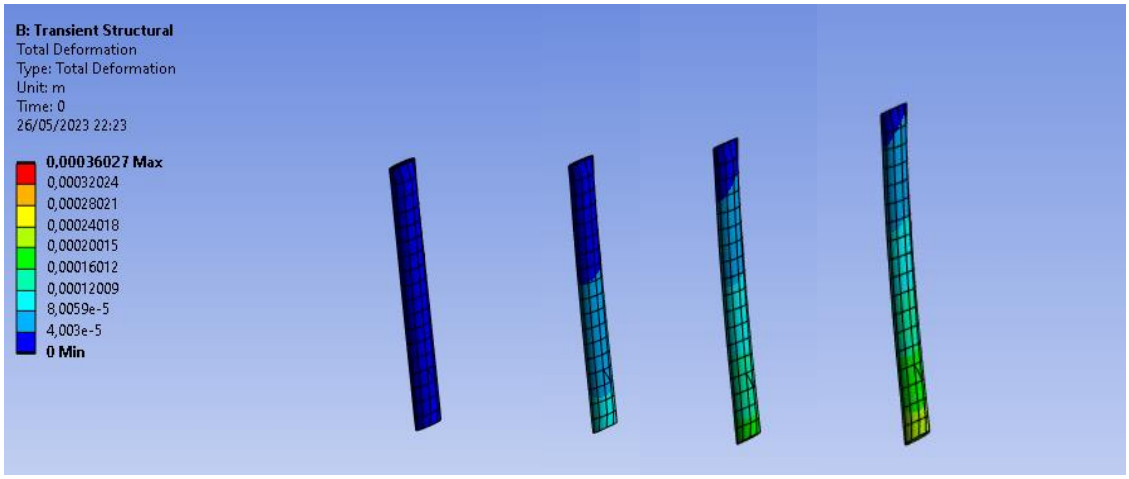

Figure 4.21: Deformation Simulation of Syrinx in the Spinal Cord

4.1.3.6 Wall Shear Deformation

The presence of the syrinx inside the central canal disrupts the normal tissue structure leading to uneven distribution of forces and strains on the surrounding tissue, resulting in higher shear strain values (see figure 4.22). This can have implications for tissue integrity, potentially leading to tissue damage, inflammation, and exacerbation of syringomyelia-related symptoms.

Negative shear strain occurs when different regions of the syrinx experience tension and compression forces. The stretching/elongation of the syrinx material along one axis can result in compression or contraction along another axis, leading to negative shear strain values. As CSF flows through the central canal and interacts with the syrinx, it exerts pressure and forces on the syrinx walls, causing it to stretch and deform (see figure 4.23).

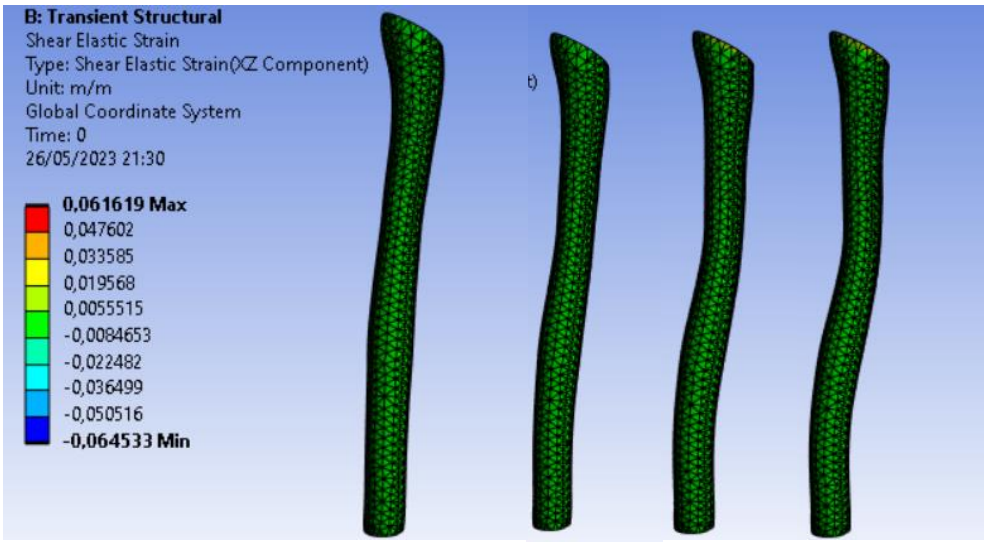

Figure 4.22: Visualization of Wall Shear Strain Distribution in the spinal cord

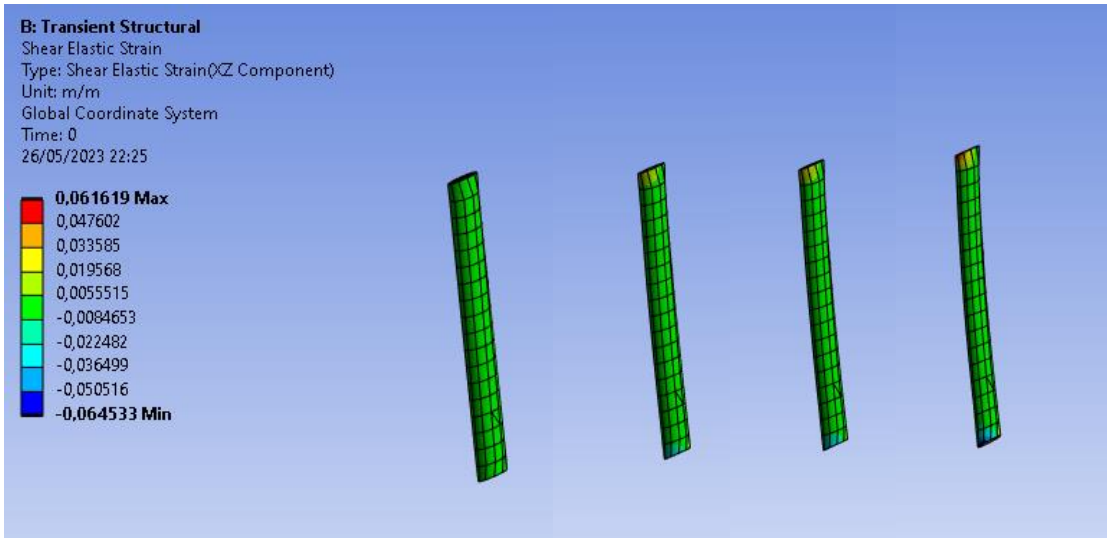

Figure 4.23: Visualization of Wall Shear Strain Distribution in Syrinx

4.3 MATLAB graphics

In order to obtain the data needed for the visualisation on MATLAB, we need to generate a report on ANSYS fluent. We will use *Surface Integrals* which is commonly used to calculate forces and moments acting on a surface or to calculate the mass flow rate, heat transfer rate, and other surface quantities. They are a way to calculate and analyse various properties of a surface in a three-dimensional space.

We are interested in visualizing the mass flow rate (see figure 4.24) as it is the rate at which fluid is flowing through a surface. It can be useful in analysing fluid flow in channels because by calculating the mass flow rate, it is possible to determine how much fluid is being transported, which can be useful for applications such as predicting the behaviour of fluids in channels.

Mass Flow Rate	[kg/s]
pres_outlet_1	-0.0089754707
velo-inlet_1	0.0093972033
Net	0.0004217326

Figure 4.24: Mass Flow Rate results

The negative value for “pres_outlet_1” indicates that the flow is leaving the domain through that surface. The positive value for “velo-inlet_1” indicates that the flow is entering the domain through that surface.

The net mass flow rate is very small, this means that there is slightly more mass is leaving the system than entering it. Because we are simulating a small region of the CSF space, a small mass flow rate could indicate that the flow is slow or limited. This could be due to factors such as narrow channels, constrictions, or blockages within the CSF space, or possibly the simulation setup itself.

The alternating pattern of increasing and decreasing mass flow rates in both the inlet and outlet (see figure 4.25 and 4.26) indicates a pulsatile flow of CSF, influenced by factors such as cardiac pulsations. The periodic nature of the flow reflects the dynamic nature of CSF movement within the system. The fact that the peak and minimum values of the mass flow rate occur at the same time for both the inlet and outlet suggests a synchronized flow pattern.

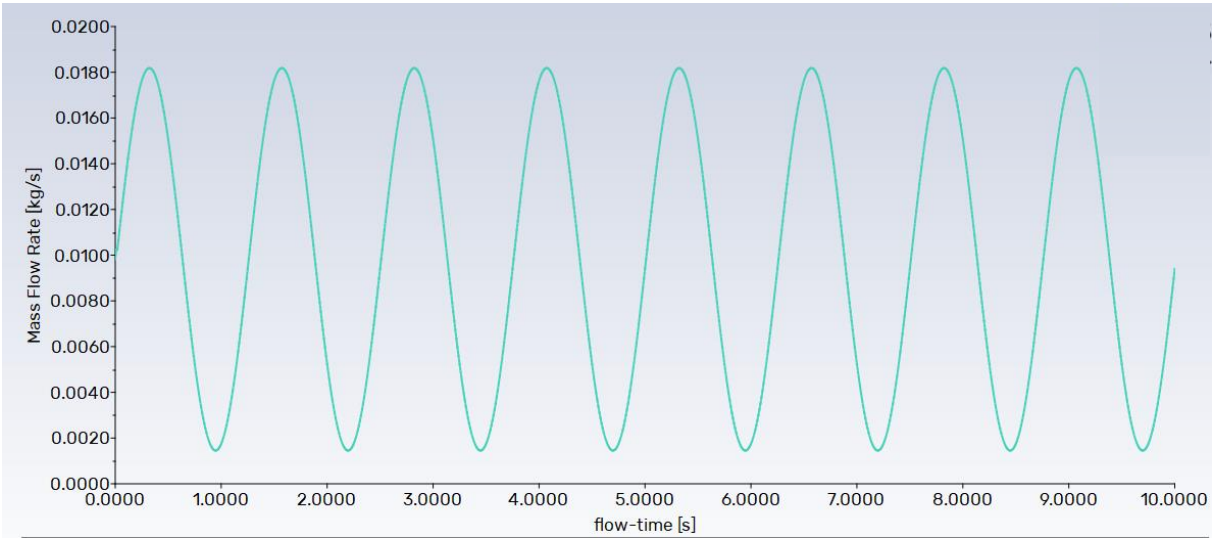

Figure 4.25: Mass Flow Rate Variation in CSF Flow Simulation: Inlet

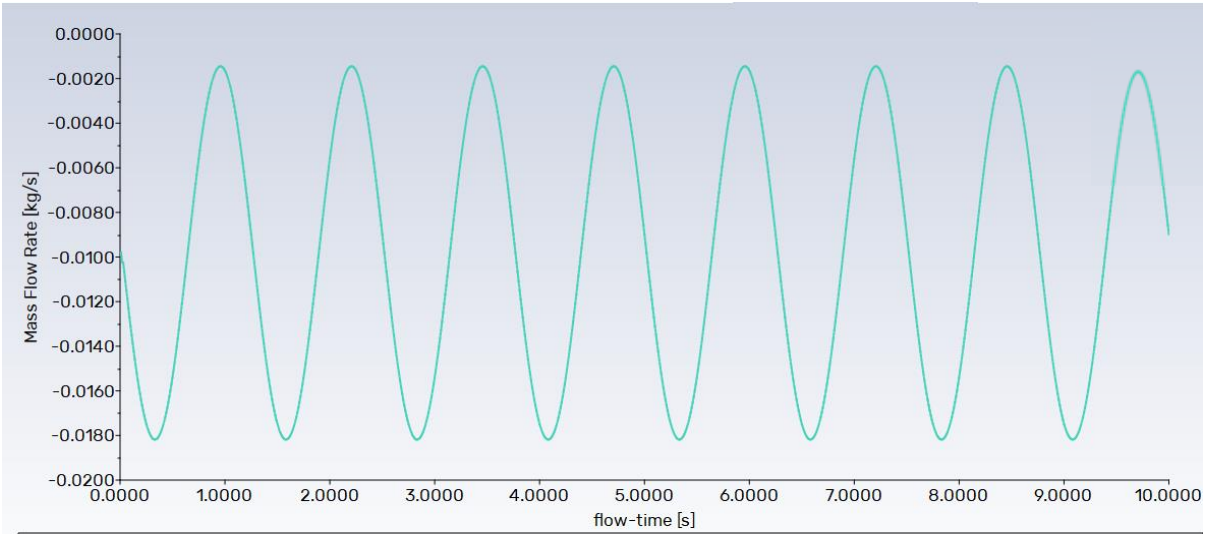

Figure 4.26: Mass Flow Rate Variation in CSF Flow Simulation: Outlet

The net flow (see figure 4.27) exhibits a similar pulsatile pattern but with reduced magnitudes compared to the individual inlet and outlet flow rates. This indicates the interplay between CSF entering and leaving the system, resulting in a net flow that oscillates around zero. This bidirectional flow is a characteristic feature of CSF circulation, which involves the continuous production, absorption, and redistribution of CSF in the central nervous system.

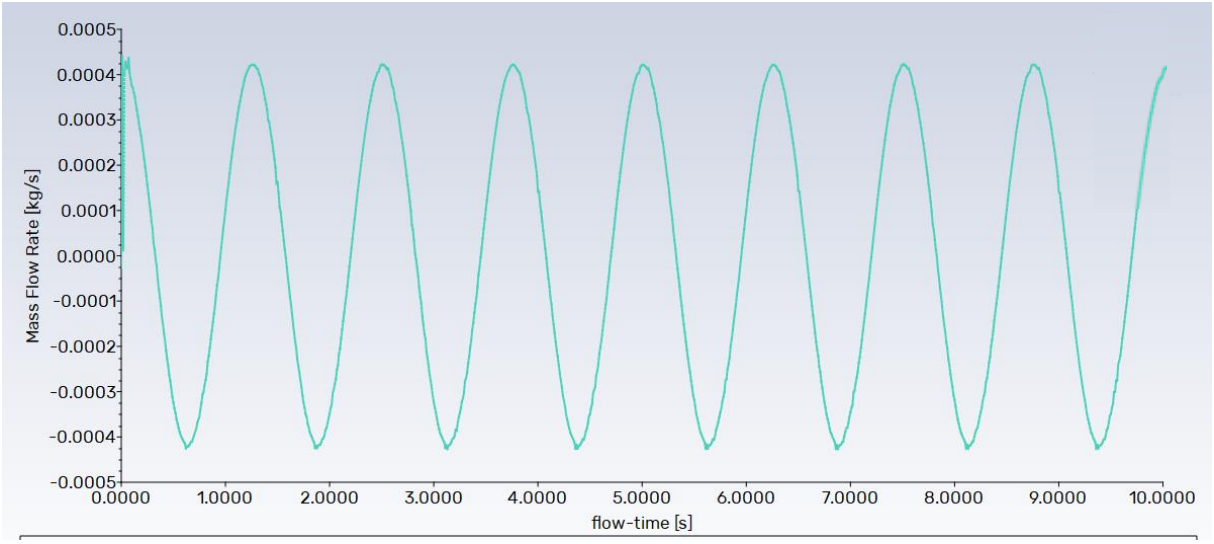

Figure 4.27: Net Flow Variation

Also by using the surface integral type set to “Area” and selecting specific surfaces, we can obtain the area of those surfaces in square meters which could be useful to represent in MATLAB (see figure 4.28). Plotting the area values on MATLAB (see figure 4.29) can give us a visual representation of the surface areas of each of the selected surfaces, which can come handy in analysing the geometry of our fluid flow system.

Besides, the mass flow rate is affected by the area, and this is because the mass flow rate is directly proportional to the flow velocity and the cross-sectional area of the fluid passage. The cross-sectional area is a geometric property that determines the flow area available for the fluid to flow through. In general, larger flow areas lead to lower fluid velocities and lower mass flow rates, while smaller flow areas lead to higher fluid velocities and higher mass flow rates. Therefore, when we calculate the area of a surface, we are indirectly estimating the available flow area.

Area	[m^2]
pres_outlet_1	0.00021570565
sas:1	0.0073688498
spinalcord:1	0.0021420929
velo-inlet_1	0.00072852535
Net	0.010455174

Figure 4.28: Area results

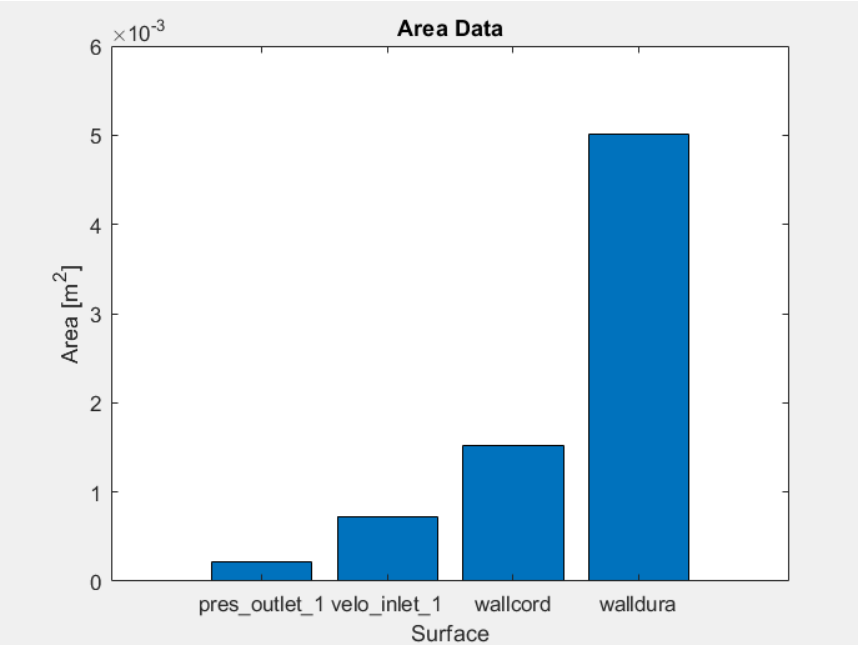

Figure 4.29: Surface Areas of Different Components in CSF Flow System

The “pres_outlet_1” bar would be the smallest, indicating that this surface has the lowest contribution to the overall mass flow rate. The “velo-inlet_1” bar would be larger than the “pres_outlet_1” bar, indicating that this surface has a higher contribution to the overall mass flow rate. The sum of “wallcord” and “walldura” would be the largest bar, indicating that the walls of the flow system (in this case, the spinal cord and duramater) contribute the most to the overall mass flow rate.

5

Discussion

The relationship between weightless conditions and syringomyelia can be explained with the alteration of the fluid-solid interactions between the spinal cord and the SAS.

Gravity plays a crucial role in regulating the flow of CSF, and changes in body position or posture affect the pressure gradient and absorption rate that also impact the function of the spinal cord (Kraus et al., 2016). According to Marshall-Goebel et al. (2020) under weightless conditions, the absence of gravity makes the CSF to be distributed more evenly. However, in a weightless environment, these flow moves more freely and results in different pressure distributions.

While we did not simulate the process of the development of a syrinx, the high-pressure gradients observed in our models 1 and 2 are consistent with the mechanical conditions thought to contribute to the occurrence and development of syringomyelia. When pressure gradients are high, it can cause CSF to accumulate in certain regions of the spinal cord, forming syrinxes. Also, deformation can also contribute to the formation of syrinxes by disrupting the normal CSF flow.

The difference in total deformation and shear stress between the three models can be attributed to the presence of the central canal and the syrinx. In the first model (spinal cord without central canal), the absence of the central canal results in a more rigid structure and when subjected to external loads or forces, the spinal cord experiences higher deformation due to limited flexibility.

In the second model (spinal cord with central canal), the presence of the central canal allows for some degree of fluid flow and movement within the canal. This fluid movement acts as a cushioning mechanism, reducing the deformation compared to the first model.

In the third model (spinal cord with central canal and syrinx), the presence of the syrinx within the central canal further alters the distribution of forces.

Some noteworthy discrepancies are seen when visualising the overall deformation of the three models in the structural transient analysis. The deformation in the first two models follows a fairly predictable pattern, with the spinal cord deforming in accordance with the applied stresses and boundary conditions.

However, there are notable differences in the deformation behaviour in the model with the syrinx. The existence of the syrinx inside the central canal can explain the expansion, thinning, and elongation of the spinal cord. As a fluid-filled cavity, the syrinx puts pressure on the spinal cord, causing it to distort and elongate.

The size and shape of the syrinx and the mechanical properties of the spinal cord, impact the extent of the deformation.

This is consistent with the characteristics of syringomyelia, in which the presence of a syrinx can cause structural alterations and spinal cord distortion. The changed deformation pattern emphasises the syrinx's influence on the mechanical behaviour of the spinal cord.

5.1 Limitations

1. The model only represents a small segment of the spinal canal and not the entire structure. This limitation means that the simulation results are not representative of the behaviour of the entire spinal canal.
2. Tissue porosity was not modelled in the study. This factor can significantly impact the fluid flow dynamics within the spinal canal and, therefore, affect the accuracy of the simulation results.
3. The brain ventricles were not included in the model. This limitation may impact the overall behaviour of the cerebrospinal fluid within the spinal canal, as the ventricles play a crucial role in the production and circulation of the cerebrospinal fluid.

The above limitations were considered to ensure that the study remains computationally feasible. Simulating the entire spinal canal, including the central canal and brain ventricles, would require a significantly larger model and higher computational power, which may not be practical. Additionally, modelling tissue porosity would require more advanced material models, which are too complex for the scope of this study.

6

Conclusions

Our study revealed important findings regarding the biomechanics of the spinal cord and the impact of a syrinx.

Examining the pressure distribution along the spinal cord, we observed a distinct gradient, gradually decreasing from high to low pressure. Interestingly, the duramater exhibited a more consistent pressure distribution throughout.

The introduction of a syrinx into the central canal disrupted the flow of CSF, leading to notable obstructions and alterations in the pathlines. These observations highlight the critical role of the central canal in modulating CSF flow dynamics.

Furthermore, our visualization of the total deformation demonstrated intriguing differences among the models. While the first two models displayed expected deformation patterns, the presence of a syrinx led to remarkable enlargement, thinning, and elongation of the spinal cord.

The mass flow rate analysis of the inlet and outlet flows uncovered cyclic variations, reflecting the dynamic balance of CSF transport. These pulsatile net flow waveforms underscore the intricate interplay between the spinal cord and CSF dynamics.

These findings contribute to our understanding of spinal cord biomechanics, emphasizing the importance of the central canal and the presence of a syrinx in syringomyelia development and occurrence. It should also be mentioned that the fluid analysis was similar in all three models.

6.1 Future lines of research

Even though our study provides insight into the effects of weightlessness on the spinal cord and its possible relation with syringomyelia, there were some limitations to our research.

Including porosity values would improve our understanding of the mechanical behaviour of the spinal cord and its interaction with surrounding tissues. If we simulated the swelling and deformation of the spinal cord, we could investigate the real development of syringomyelia.

Another area of future investigation is to expand our model to include the cerebral ventricular system. This would give us a more complete picture of the complex interactions between these structures and their effects on the spinal cord.

Also expanding this study by including simulations with normal gravity values would show a better understanding of the role of gravity in the development of syringomyelia.

7

Conclusiones

Nuestro estudio reveló aspectos importantes sobre la biomecánica de la médula espinal y el impacto de una siringe (quiste lleno de líquido):

Al examinar la distribución de presión a lo largo de la médula espinal, observamos un gradiente que disminuye gradualmente desde una presión alta hasta una baja. Curiosamente, la duramadre mostró una distribución de presión más consistente.

La introducción de una siringe en el canal central interrumpió el flujo de líquido cefalorraquídeo (LCR), causando obstrucciones y alteraciones en los patrones de flujo. Estas observaciones resaltan el papel crítico del canal central en la modulación de la dinámica del flujo de LCR.

Además, nuestra visualización de la deformación total reveló diferencias intrigantes entre los tres modelos. Mientras que los dos primeros mostraron patrones de deformación esperados, la presencia de una siringe condujo a un notable aumento de tamaño, adelgazamiento y elongación de la médula espinal.

El análisis del caudal en las entradas y salidas reveló variaciones cíclicas, reflejando el equilibrio dinámico en el transporte del LCR. Estas formas de onda pulsátiles de flujo neto subrayan la compleja interacción entre la médula espinal y la dinámica del LCR.

Estos hallazgos contribuyen a la comprensión de la biomecánica de la médula espinal, enfatizando la importancia del canal central y la presencia de una siringe en el desarrollo y aparición de la siringomielia. Cabe destacar que el análisis del fluido, CSF, fue similar en los tres modelos.

7.1 Futuras líneas de trabajo

Aunque nuestro estudio proporciona información sobre los efectos de la ingravidez en la médula espinal y su posible relación con la siringomielia, hubo algunas limitaciones.

Incluir valores de porosidad mejoraría nuestra comprensión del comportamiento mecánico de la médula espinal y su interacción con los tejidos circundantes.

Si simuláramos la inflamación de la médula espinal, podríamos investigar el desarrollo real de la siringomielia.

Otra futura línea de trabajo sería ampliar nuestro modelo para incluir los ventrículos cerebrales. Esto nos daría una imagen más completa de las interacciones complejas entre estas estructuras y sus efectos en la médula espinal.

Además, ampliar este estudio mediante la inclusión de simulaciones con valores normales de gravedad permitiría una mejor comprensión del papel de la gravedad en el desarrollo de la siringomielia.

Bibliography

Di Terlizzi R, Platt S. The function, composition and analysis of cerebrospinal fluid in companion animals: part I - function and composition. Vet J. 2006 Nov;172(3):422-31. doi: 10.1016/j.tvjl.2005.07.021. Epub 2005 Sep 9. PMID: 16154365.

Haines, D.E. and Mihailoff, G.A. (2019) *Principios de neurociencia: Aplicaciones Básicas y Clínicas*. Barcelona, España: Elsevier.

Stienen MN, Cadosch D, Seule MA, Hildebrandt G, Heilbronner R, Gautschi OP. Die Adulte Syringomyelie - ein Krankheitsbild mit Verschiedenen Ursachen [Adult syringomyelia - a syndrome of different origins]. Praxis (Bern 1994). 2011 Jun 8;100(12):715-25. German. doi: 10.1024/1661-8157/a000564. PMID: 21656499.

Michael L. Sternberg, Michael L. Gunter,Syringomyelia,The Journal of Emergency Medicine, Volume 53, Issue 2, 2017, Pages e31-e32, ISSN 0736-4679, doi:10.1016/j.jemermed.2017.04.029.

Fillingham, P., Rane Levendovszky, S., Andre, J., Parsey, C., Bindschadler, M., Friedman, S., et al. (2022). Patient-specific computational fluid dynamic simulation of cerebrospinal fluid flow in the intracranial space. Brain Res. 1790, 147962. doi:10.1016/j.brainres.2022.147962

Kyriakou, E. (2006). The biomechanics of syringomyelia. https://unsworks.unsw.edu.au/entities/publication/9a4b6d44-d22d-49ae-bf6a-ba6fbd61efef

Lawley, J. S., Petersen, L. G., Howden, E. J., Sarma, S., Cornwell, W. K., Zhang, R., Whitworth, L. A., Williams, M., & Levine, B. D. (2017). Effect of gravity and microgravity on intracranial pressure. The Journal of Physiology, 595(6), 2115–2127. https://doi.org/10.1113/jp273557

Cinalli, G., Özek, M. M., & Sainte-Rose, C. (2019). Pediatric Hydrocephalus. Springer Publishing.

Brinker, T. (2014, May 1). A new look at cerebrospinal fluid circulation - Fluids and Barriers of the CNS. BioMed Central. https://fluidsbarrierscns.biomedcentral.com/articles/10.1186/2045-8118-11-10

Adigun, O. O., & Al-Dhahir, M. A. (2019). Anatomy, Head and Neck, Cerebrospinal Fluid. StatPearls Publishing, Treasure Island (FL) EBooks. https://pubmed.ncbi.nlm.nih.gov/29083815/

Di Terlizzi, R., & Platt, S. (2006). The function, composition and analysis of cerebrospinal fluid in companion animals: Part I – Function and composition. The Veterinary Journal, 172(3), 422-431. https://doi.org/10.1016/j.tvjl.2005.07.021

Orešković, D., Radoš, M., & Klarica, M. (2017). Role of choroid plexus in cerebrospinal fluid hydrodynamics. Neuroscience, 354, 69–87. https://doi.org/10.1016/j.neuroscience.2017.04.025

J.J. Kaneko, J.W. Harvey, M.L. Bruss (Eds.), Clinical Biochemistry of Domestic Animals, Academic Press, New York (1997), pp. 785-827

Idris, Z. (2014). Searching for the Origin through Central Nervous System: A Review and Thought which Related to Microgravity, Evolution, Big Bang Theory and Universes, Soul and Brainwaves, Greater Limbic System and Seat of the Soul. The Malaysian Journal of Medical Science, 21(4), 4–11.

Telano, L. N., & Baker, S. (2022). Physiology, Cerebral Spinal Fluid. In StatPearls. StatPearls Publishing.

Cousins, O., Hodges, A., Schubert, J., Veronese, M., Turkheimer, F., Miyan, J. A., Engelhardt, B., & Roncaroli, F. (2021). The blood–CSF–brain route of neurological disease: The indirect pathway into the brain. Neuropathology and Applied Neurobiology, 48(4). https://doi.org/10.1111/nan.12789

Deng, S., Gan, L., Liu, C., Xu, T., Zhou, S., Guo, Y., Zhang, Z., Yang, G., Tian, H., & Tang, Y. (2022). Roles of Ependymal Cells in the Physiology and Pathology of the Central Nervous System. *Aging and Disease*, 0. https://doi.org/10.14336/ad.2022.0826-1

Nelles, D. G., & Hazrati, L. (2022). Ependymal cells and neurodegenerative disease: outcomes of compromised ependymal barrier function. Brain Communications, 4(6). https://doi.org/10.1093/braincomms/fcac288

Kumar, V., Umair, Z., Kumar, S., Goutam, R. S., & Park, S. (2021). The regulatory roles of motile cilia in CSF circulation and hydrocephalus. Fluids and Barriers of the CNS, 18(1). https://doi.org/10.1186/s12987-021-00265-0

Jiménez, A. M., Domínguez-Pinos, M. D., Guerra, M. E., Fernández-Llebrez, P., & Pérez-Fígares, J. M. (2014). Structure and function of the ependymal barrier and diseases associated with ependyma disruption. Tissue Barriers, 2(1), e28426. https://doi.org/10.4161/tisb.28426

Fanous, R., & Midia, M. (2007). Perivascular Spaces: Normal and Giant. THE CANADIAN JOURNAL OF NEUROLOGICAL SCIENCES, 34(1), 5–10. https://doi.org/10.1017/s0317167100005722

Mestre, H. (2018, November 19). Flow of cerebrospinal fluid is driven by arterial pulsations and is reduced in hypertension. Nature. https://www.nature.com/articles/s41467-018-07318-3?error=cookies_not_supported&code=1c268339-c240-4721-8e10-cf0384f10b12

Greitz, D., Wirestam, R., Franck, A., Nordell, B., Thomsen, C., & Ståhlberg, F. (1992). Pulsatile brain movement and associated hydrodynamics studied by magnetic resonance phase imaging. Neuroradiology, 34(5), 370–380. https://doi.org/10.1007/bf00596493

Zahid, A., Martin, B. A., Collins, S., Oshinski, J. N., & Ethier, C. R. (2021). Quantification of arterial, venous, and cerebrospinal fluid flow dynamics by magnetic resonance imaging under simulated micro-gravity conditions: a prospective cohort study. Fluids and Barriers of the CNS, 18(1). https://doi.org/10.1186/s12987-021-00238-3

NHS website. (2022, November 11). Chiari malformation. nhs.uk. https://www.nhs.uk/conditions/chiari-malformation/

Holly, L. T., & Batzdorf, U. (2019). Chiari malformation and syringomyelia. Journal of Neurosurgery: Spine, 31(5), 619–628. https://doi.org/10.3171/2019.7.spine181139

Chiari Malformation – Symptoms, Diagnosis and Treatments. (n.d.). https://www.aans.org/en/Patients/Neurosurgical-Conditions-and-Treatments/Chiari-Malformation

Chiari malformation: Non-surgical alternatives to Chiari decompression surgery – Caring Medical Florida. (n.d.). https://www.caringmedical.com/prolotherapy-news/chiari-malformation-non-surgical-alternatives-chiari-decompression-surgery/

Stoodley, M. A., Jones, N. C., Yang, L., & Brown, C. (2000). Mechanisms underlying the formation and enlargement of noncommunicating syringomyelia: experimental studies. Neurosurgical Focus, 8(3), 1–7. https://doi.org/10.3171/foc.2000.8.3.2

Shafique, S. (2022, August 8). Anatomy, Head and Neck, Subarachnoid Space. StatPearls - NCBI Bookshelf. https://www.ncbi.nlm.nih.gov/books/NBK557521/

Farb, R. I., & Rovira, A. (2020). Hydrocephalus and CSF Disorders. In IDKD Springer series (pp. 11–24). Springer International Publishing. https://doi.org/10.1007/978-3-030-38490-6_2

National Organization for Rare Disorders. (2023, January 12). Arachnoid Cysts - Symptoms, Causes, Treatment | NORD. https://rarediseases.org/rare-diseases/arachnoid-cysts/

Verhaagen, J., & McDonald, J. W. (2012). Spinal Cord Injury. Elsevier Gezondheidszorg.

Leclerc, A., Matveeff, L., & Emery, E. (2021). Syringomyelia and hydromyelia: Current understanding and neurosurgical management. Revue Neurologique, 177(5), 498–507. https://doi.org/10.1016/j.neurol.2020.07.004

Squire, L. R. (2008). Encyclopedia of Neuroscience (1st ed.). Academic Press.

Milhorat, T. H. (2000). Classification of syringomyelia. Neurosurgical Focus, 8(3), 1–6. https://doi.org/10.3171/foc.2000.8.3.1

Syringomyelia. (2022, June 27). MedLink Neurology. https://www.medlink.com/articles/syringomyelia

Williams, H. (2008, April 11). A unifying hypothesis for hydrocephalus, Chiari malformation, syringomyelia, anencephaly and spina bifida - Fluids and Barriers of the CNS. BioMed Central. https://fluidsbarrierscns.biomedcentral.com/articles/10.1186/1743-8454-5-7

Williams, B. (1980). On the Pathogenesis of Syringomyelia: A Review. Journal of the Royal Society of Medicine, 73(11), 798–806. https://doi.org/10.1177/014107688007301109

Pillay, P. K., Awad, I. A., & Hahn, J. F. (1992). Gardner's hydrodynamic theory of syringomyelia revisited. Cleveland Clinic Journal of Medicine, 59(4), 373–380. https://doi.org/10.3949/ccjm.59.4.373

Ma, Y., Zhao, X., Ye, X., Jiang, N., & Zhou, J. (2020). A transient fluid–structure interaction analysis strategy and validation of a pressurized reactor with regard to loss-of-coolant accidents. Nuclear Science and Techniques. https://doi.org/10.1007/s41365-020-00771-0

Martin, B. A., Kalata, W., Shaffer, N., Fischer, P., Luciano, M. G., & Loth, F. (2013). Hydrodynamic and Longitudinal Impedance Analysis of Cerebrospinal Fluid Dynamics at the Craniovertebral Junction in Type I Chiari Malformation. PLOS ONE, 8(10), e75335. https://doi.org/10.1371/journal.pone.0075335

Lever, M. J. (2005b). Mass transport processes in artificial organs. Elsevier EBooks, 153–166. https://doi.org/10.1533/9781845690861.3.153

Thomas, J. M. (2019). Fluid dynamics of cerebrospinal fluid flow in perivascular spaces. Journal of the Royal Society Interface, 16(159), 20190572. https://doi.org/10.1098/rsif.2019.0572

A Poroelastic Model of Spinal Cord Cavities. (n.d.). The University of Brighton. https://research.brighton.ac.uk/en/studentTheses/a-poroelastic-model-of-spinal-cord-cavities

Martin, B. A., Kalata, W., Loth, F., Royston, T. J., & Oshinski, J. N. (2005). Syringomyelia Hydrodynamics: An In Vitro Study Based on In Vivo Measurements. *Journal of Biomechanical Engineering*, *127*(7), 1110–1120. https://doi.org/10.1115/1.2073687

Rusbridge, C., Greitz, D., & Iskandar, B. J. (2006). Syringomyelia: Current Concepts in Pathogenesis, Diagnosis, and Treatment. *Journal of Veterinary Internal Medicine*, *20*(3), 469–479. https://doi.org/10.1111/j.1939-1676.2006.tb02884.x

Liu, X., Luo, D., Hu, P., Yu, M., & Rong, Q. (2017). Modelling and Analysis of the Cerebrospinal Fluid Flow in the Spinal Cord. *Communications in Computer and Information Science*. https://doi.org/10.1007/978-981-10-6370-1_8

Alperin, N., Lee, S. Y., Loth, F., Raksin, P. B., & Lichtor, T. (2000). MR-Intracranial Pressure (ICP): A Method to Measure Intracranial Elastance and Pressure Noninvasively by Means of MR Imaging: Baboon and Human Study. Radiology, 217(3), 877–885. https://doi.org/10.1148/radiology.217.3.r00dc42877

15.2. Transient Analysis. (2017, July 14). https://www.mm.bme.hu/~gyebro/files/ans_help_v182/ans_thry/thy_anproc2.html

Koizumi H, Yamanaka K, Kinoshita M, et al. Syringomyelia in spinal cord injury. Spinal Cord. 2019;57(11):903-907. doi:10.1038/s41393-019-0288-0

Gazenko, O. G., Grigoriev, A. I., Egorov, A. D., & Barer, R. G. (1981). Problems of gravitational physiology in manned space flight. Acta Astronautica, 8(9-10), 1127-1140.

Appendix

```c
#include "udf.h"
#define PI 3.141592654

DEFINE_PROFILE(csf_velocity, thread, index)
{
  face_t f;
  real t = CURRENT_TIME;
  real peak_vel = 0.025;
  real min_vel = 0.002;
  real period = 1.25;
  real amplitude = (peak_vel - min_vel) / 2.0;
  real velocity = (peak_vel + min_vel) / 2.0 + amplitude * sin((2.0 * PI / period) * t);

  begin_f_loop(f, thread)
  {
    F_PROFILE(f, thread, index) = velocity;
  }
  end_f_loop(f, thread)
}
```

Image A. UDF function used on Ansys Fluent

```matlab
% Define the area data
areaData = [0.0002160563, 0.00072885301, 0.0015253923, 0.005010874];

% Define the labels for each bar
barLabels = {'pres\_outlet\_1', 'velo\_inlet\_1', 'wallcord', 'walldura'};

% Create a bar plot
bar(areaData)

% Set the x-axis tick labels
xticklabels(barLabels)

% Add a title and axis labels
title('Area Data')
xlabel('Surface')
ylabel('Area [m^2]')
```

Image B. Matlab code

UNIVERSIDAD DE MÁLAGA | uma.es

E.T.S. DE INGENIERÍA INFORMÁTICA

E.T.S de Ingeniería Informática
Bulevar Louis Pasteur, 35
Campus de Teatinos
29071 Málaga